AFRICA CENTER OF EXCELLENCE FOR WATER MANAGEMENT

ADDIS ABABA UNIVERSITY

Evaluating the Land Use and Land Cover Change Impact on Streamflow, Kulfo Catchment

M.Sc. THESIS

By

Assebe Anja

Advisor: - Dr. Ing Adane Abebe

October, 2021

ACEWM/AAU, ETHIOPIA

Evaluating the Land Use and Land Cover Change Impact on Streamflow, Kulfo Catchment

BY

ASSEBE ANJA ALEMU

A THESIS SUBMITTED TO THE DEPARTMENT OF HYDROLOGY AND WATER RESOURCES, SCHOOL OF POSTGRADUATE STUDIES, AFRICAN CENTER OF EXCELLENCE FOR WATER MANAGEMENT (ACEWM)/ ADDIS ABABA UNIVERSITY (AAU) IN PARTIAL FULFILLMENT OF THE REQUIREMENTS FOR THE DEGREE OF MASTER OF SCIENCE IN WATER MANAGEMENT SPECIALIZATION OF HYDROLOGY AND WATER RESOURCES.

October, 2021

ACEWM/AAU, ETHIOPIA

ADVISOR THESIS SUBMISSION APPROVAL SHEET

SCHOOL OF GRADUATE STUDIES

AFRICA CENTER OF EXCELLENCE FOR WATER MANAGEMENT

ADDIS ABABA UNIVERSITY

This is to certify that the thesis entitled **"Evaluating the Land Use and Land Cover Change Impact On Streamflow, Kulfo Catchment "** submitted in partial fulfillment of the requirements for the degree of Master's with specialization in Hydrology and Water Resources, the Graduate Program of the Water management and has been carried out by Mr. ASSEBE ANJA under my supervision. Therefore, I confirm that the student has fulfilled the requirements and hence hereby can submit the thesis to the department for defense.

Dr.Ing Adane Abebe

(Advisor)

12/10/2021

Date

Approval Page

This thesis proposal entitled "**Evaluating the Land Use and Land Cover Change Impact On Streamflow, Kulfo Catchment ''** is approved by Advisor, Examiners, and Head of Africa Center of Excellence for Water Management for partial fulfillment of the requirement for Master of Science in Water Management Specialization of Hydrology and Water Resources.

Submitted by:

Assebe Anja Alemu	……	……
Name	Signature	Date

Thesis approval by:

Dr.Ing Adane Abebe	……	....12/10/2021…
(Principal Advisor)	Signature	Date
Chairperson		
Dr.Getachew Dagnew	…..…….……	…..……
	Signature	Date
Examiner		
Professor Tenalem Ayenew	……...	……
	Signature	Date
Dr.Getachew Tegegne	……...	……
	Signature	Date
Dr. Feleke Zewge	…….....	……
(Head of ACEWM)	Signature	Date
Netsanet Assefa (M.Sc)	……	…….
(Coordinator)	Signature	Date

DECLARATION

I, Assebe Anja Alemu, declared this thesis as it's my original work. This has not been presented in any university before and will not be present to any other university by me or anyone to award similar or any other degree.

_____

Signature

ACKNOWLEDGEMENT

First of all, I would like to thank God, the source of all knowledge, the owner of heaven and earth, for his priceless and miracle gifts to me because without him I would not do it.

I would also wish to express my sincere gratitude to my advisor, Dr.Ing Adane Abebe, for his willingness to work with me, for his kindness, and his patience, constructive ideas, and more.

I gratefully acknowledge all offices and personalities who have provided me the necessary data for my study: Ministry of Water, Irrigation and Energy, National Metrological Service Agency and Ethiopian Geospatial institute.

I would like to express my sincere gratitude to the African Center of Excellence for Water Management for providing a variety of learning materials, covering the research cost, and responding quickly to my questions as well as the staff members of the Center.

My heartfelt thanks go to Arba Minch University for permitting and sponsoring me to follow this Master of Science Program in Hydrology and Water Resources Management.

I would wish to thank my classmates, especially Mr. Tilaye Worku and Mr. Abdisa Sime for their invaluable support, advice, kindness, and sincerity. I appreciate their encouragements, comments, motivations and the inspirations of these two guys that makes me to conduct and finish this thesis work on time and in advance.

I wish to extend my gratitude to my family for their love, constant moral support, and ultimate support throughout my thesis work.

ABSTRACT

Streamflow is one of the key components of the hydrological cycle that can be altered and/or modified by a variety of variables. One of the key variables is the change in LULC. In kulfo cathement, in Ethiopia's southern region, suitable LULC detection techniques were not addressed and evaluated yet, and also the changing of the exesting LULC is the main stress in the streamflow of the Kulfo catchment. As a result, the impact of LULC change on streamflow was assessed in this study using the soil and water assessment tool model. Sensitivity, calibration, and validation were also performed using historical streamflow data in SWAT-CUP (Calibration and Uncertainty program) using sequential uncertainty fitting–version 2 (SUFI-2). There were four different algorithms applied to classify the LULC change. The best performing of four distinct algorithms (SVM, CART, RF, and Navia's) available in the Google Earth Engine were compared, and the best performing was chosen to generate the time-series LULC maps of the research area (1986, 2000, 2016, and 2020). GCPs gathered in the field were used to assess the accuracy of these algorithms. To train and evaluate the LULC maps generated from the Google Earth Engine platform, high resolution (30m) Landsat imagery from the thematic mapper (TM), enhanced thematic mapper plus (ETM+), and operational land imager (OLI) were employed, along with historical trends and ground-based data. As a result, the SVM method outperformed the other algorithms in this study when it came to LULC classification. During the study's period, the area covered by vegetation declined from 18.81 % to 3.1 %, while agricultural land increased from 19.44 % to 57.12 % and shrub land decreased from 34.18 % to 14.73 %. As a result, the impact of these LULC variations on streamflow was assessed using the Soil & Water Assessment Tool (SWAT) model, and over the study's period, substantial mean monthly and seasonal streamflow variability was observed. Monthly, these variabilities were raised from 6.72 % to 7.85%. The year has been divided in to three seasons Kiremt, Belg, and Bega. Seasonally, streamflow has dropped for all seasons (Kiremt, Belg, and Bega) from 2016 to 2020, but it has increased from 2000 to 2016. (Kiremt, Belg, and Bega). The calibration results showed an acceptable range between observed and simulated streamflow (0.6, 0.8, 0.75, and 0.75 for NSE and 0.75, 0.76, 0.79, and 0.81 for R2). Validation findings for observed and simulated streamflow were similarly within acceptable limits (0.72, 0.6, 0.74, and 0.75 for NSE and 0.8, 0.75, 0.73, and 0.8 for R2).

Keywords: Google Earth Engine, Streamflow, SWAT, SWAT-CUP, Machine Learning, Kulfo

TABLE OF CONTENTS

ABBREVIATIONS AND ACRONYMS

API	Application Programming Interface
DEM	Digital elevation model
EMA	Ethiopian Meteorological Agency
GEE	Google earth engine
FAO	Food and agricultural organizations
GIS	Geographical information system
GPS	Geographical positioning system
HRU	Hydrological response units
LULU	Land use land cover
M^3 /s	Cubic meter per second
MOWIE	Ministry of Water Irrigation and Electricity
NMA	National Meteorological Agency
NSE	Nash Sutcliffe simulation efficiency
OLI	Operational Land Imager
R^2	Coefficient of determination
SWAT	Soil and water assessment tool
SWAT-CUP	Soil and water assessment tool calibration and uncertainty programs

LIST OF FIGURES

LIST OF TABLES

LIST OF APPENDIX

1. INTRODUCTION

1.1 Background

Water resources are vital renewable resources that are necessary for life and contribute to a society's socioeconomic growth (Destaa & Lemma, 2017). However, the depletion of water resources has turned into a major environmental issue (Ayana, Chemeda, & Ekasit, 2012). As a result, optimal exploitation of these resources necessitates both geographical and temporal assessment and management of the quantity and quality of water resources.

Land is also the main type of natural resource on which many human activities are carried out, such as agriculture, forest removal for settlement, and infrastructure construction. As a result of this activity, the availability of various natural resources, such as vegetation, land fertility, soil, and water, is impacted. In addition, it has a direct impact on evapotranspiration, groundwater infiltration, and runoff (Fisseha et al., 2011; Tewabe and Fentahun, 2020).

Land use and land cover changes have occurred throughout history, are now occurring, and are expected to continue in the future. For thousands of years, human actions have altered the ecosystem (Fisseha et al., 2011).

According to Roy (2010), changing land use and land cover has an impact on vegetation by diminishing its coverage, which leads to biodiversity loss, erosion of natural soil, and the availability of ground and surface water. It also has a detrimental impact on an area's prospective usage and can lead to soil degradation and loss, as well as pollution of water, soil, and air (Tegene, 2002; Alemu, 2015; Geetha, et al., 2019).

Several phenomena linked with the natural circulation of water are included in hydrological processes. The separation of precipitated water into either infiltration into the soil or runoff generation is one of these occurrences (Loewen and Pinheiro, 2017).

Streamflow is an important hydrological variable for water resource planning and management as well as ecosystem conservation (Khalid et al., 2017).

Infiltration, erosion, and evapotranspiration are all affected by LUCC, which is a key characteristic in the runoff process. To understand the future effects of land use and land cover on streamflow at the watershed level, it is necessary to first understand the consequences of historic LULC changes on river flow. Significant effects on hydrological cycles and subsequent repercussions on water supplies are projected as a result of these changes. (Githu, 2009).

The baseline data for a better understanding of how the land was utilized in the past and what forms of change are projected in the future is provided by the LULC change analysis. LULC change studies also provide useful data for analyzing the environmental effects of human activities on climate change, streamflow, and other factors. (Tegene, 2002).

The altering effects of LULC on natural resources are becoming increasingly seen around the world (Berihun, et al., 2019). Due to population pressure, relocation schemes, climate change, and other human and natural-induced driving forces, particularly Ethiopia has experienced rapid changes (Marchant, et al., 2018).

Generally, Changes in LULC have a wide range of effects on environmental and landscape variables, including water, land, and air quality, ecosystem processes, and functions (Rimal, 2011). Therefore, combining remote sensing data and analysis methodologies to investigate the changing gives reliable, timely, and detailed information for monitoring changes in land use and land cover.

Satellite images span a large area, and the data from them can be retrieved and processed fast on a computer. Many important and valuable information connected to many applications such as land cover, air quality, disaster management, urban planning, weather forecast, and so on can be interpreted with only a single image taken from the satellite sensor. As a result, the majority of land resource management research is centered on satellite image processing (Uddin et al., 2018).

For processing, exploiting, and executing complicated calculations on historical global-scale satellite imagery, Google Earth Engine (GEE), an open-access cloud-based computing platform, is being employed. Furthermore, powerful machine learning algorithms which are available on GEE enable scientific analysis and visualization of geospatial datasets. (Wagle et al., 2020; Google EarthEngine, 2012; Isabela Xavier Floreano, 2021).

Various models have been developed and applied to predict, assess, and monitor natural phenomena such as streamflow and sediment yield from the catchment, but the SWAT model, which is a deterministic, continuous watershed model that can operate on daily and hourly time steps, is the most widely used and freely available.

According to Jha (2011), the SWAT model is the best of the hydrological models because of its ability to apply to large-scale watersheds (> 100 km2), interface with a Geographic Information System (GIS), continuous-time simulations performance, generation of the

largest number of sub-basins, and ability to characterize the watershed in sufficient spatial detail.

1.2 Statement of the Problem

LULC dynamics is one of the foremost causes of land degradation, including deforestation and deterioration of soil and water quality and quantity, the decline in natural resources base, and ultimately the disruption of hydrology cycle such as infiltration, interception, erosion, and evapotranspiration (Rindfuss et al, 2004). High irrigation activity, land degradation, expansion of agriculture field and different activities were dominated in the caple of the decade for the case of Kulfo catchment. The catchment has been continuously used for agricultural purposes and different land features have been changed to cropland (Ashebir, 2018). These land use and land cover change have caused a lot of tension in the streamflow.

Kulfo River has crucial importance to the natural habitats of Abaya - Chamo basin as well as other land users in the catchment. Major environmental problems such as the changing of land use and land cover have been observed in recent years this in return alters the water availability, causes erosive landscapes, and low soil nutrients (Teshome, 2020).

Therefore, Understanding how these activities influence streamflow will enable planners to formulate policies towards minimizing the undesirable effects of future land-use and land cover changes on the hydrology of the river so that the hydrological cycle will not be significantly alerted. Besides planners local farmers will benefit more as well as researchers will gain fruitful knowledge. Therefore, the need for scientific research to minimize the impact of land use and land cover change on the streamflow of Kulfo catchment is essential.

Even if a lot of studies have been conducted on Kulfo catchment like model comparison on the performance of Rainfall-Runoff modeling (Abyot, 2008); the impact of climate change on kulfo river (Nega *et al*., 2018; Tadelech, 2015) and land use and land cover changes and their effects on the landscape of Abaya-Chamo basin (Yohannes *et al*., 2018).

Most researches have limitations on producing and quantifying dynamics of LULC map effects on stream flow. This limitation occurs in applying an appropriate classification algorithm for LULC classification. For instance (Neetu & Ray, 2019) classified land use land cover features and used RF classifier which is available on GEE with comparing it with other types of classifier just by assessing the accuracy depending on collected training data on the platform rather than using GCS.

1.3 Objective of the Study

Main Objective

The main objective of the study was to evaluate the land use land cover change impact on streamflow for the case of Kulfo catchment.

Specific Objectives

1. To evaluate the machine learning algorithms (classifier) for LULC classification.
2. To identify the main historical LULC class and their change as well as sensitive parameters for streamflow generation.
3. To assess the streamflow trends over the historical period (1986 to 2020)

1.4 Research Questions

Based on the research objectives the following research questions were formulated.

- Which machine learning classifier is appropriate for the classification of land use and land cover for kulfo catchment?
- What are the main land use and land cover types and their areal coverage in kulfo catchment and the most sensitive parameters for the generation of streamflow?
- How do land use and land cover affect (impacts) streamflow of Kulfo Catchment?

1.5 Scope of the Study

This study is limited to analyzing LULC change impacts on stream inflow in kulfo, catchment. And hydrologic modeling has been done using the SWAT model incorporated with GIS. The LULC change and map were identified using the google earth engine application for the periods of 1986, 2000 2016, and 2020. Furthermore, using these maps the streamflow has been modeled. This study only focuses on the impact of LULC change on streamflow.

1.6 Significance of the Study

The main significance of this study is understanding the impacts of LULC change on natural resources, streamflow so that its impact will be reduced and the findings of this study will give scientific clues for resource base analysis and development of effective and appropriate response strategies for sustainable management of natural resources. Currently, a lot of infrastructures are under building around the riparian of the river, kulfo, like recreational areas, water pumping wells to agricultural land, therefore, the result of this study will give a better understanding to consider changing amount and types of LULC on the catchment so that they can consider it.

2. LITERATURE REVIEW

2.1. Overview of land use and land cover change

Land is the biosphere's ultimate resource, and it has been changing for decades as a result of human and natural influences. The phrases "land use" and "land cover" have different meanings.

Land cover refers to the visible physical characteristics of the Earth's surface, such as water bodies and vegetation, as well as those created by human activities, such as settlement areas, agricultural lands, urbanized land features, exposed land surface due to tree removal for plantation, and others. (Gregorio, 2000).

Land use, on the other hand, refers to the physical future of the earth as it is used by humans and their homes (such as agriculture, settlements, industry, etc.) (Harshika et al., 2012; Sabzar et al., 2016).

Farda, (2017); Lunetta, (2006) defined land use as a human endeavor to alter the future of land to create a favorable environment for their lives by engaging in various activities such as agricultural land, road construction, and settlement. Environmental issues, according to the author, are tied to land-use change. Therefore, LULC change analysis is required for environmental management through decision-making and future planning.

Conversion or modification of land characteristics can result in changes in land use and land cover (Lambin, 2003). Sun, Liu, & Sha, (2016), define conversion as the process of changing from one cover or use type to another, whereas modification is the process of maintaining the broad cover or use type in the face of changes in its attributes (Yoon, 2011).

Generally, Land use and land cover change refer to the changing of the earth's terrestrial surface caused by natural or manmade activities (Dinka and Chaka, 2019). Changes in land use and land cover are major components of global environmental change, and they affect the earth's system's functionality directly or indirectly (Ganasri, 2015).

2.2. Causes of land-use and land-cover changes

Examining the mechanisms that drive LULC change is critical in solving environmental problems. Various complicated elements that influence specific environmental, economic, and social situations are responsible for the transformation. Interactions of social, political, economic, demographic, technical, cultural, and biophysical elements may shape the driving forces of LULC change (Msofe, Sheng, & Lyimo, 2019).

The factors that lead to changing of the LULC are broadly categorized as anthropogenic and natural factors. However, anthropogenic factors such as increased settlement associated with population growth, industrial development, irrigation, and urban growth (Ochuka et al., 2019) as well as developments, expansion of agricultural land and town (Rowcroft, 2005), deforestation, resettlements, shifting of cultivation, and forest fire are all factors that lead to changes in the LULC (Emiru et al., 2018).

In a study conducted by Emiru et al., (2018) on bambasi wereda, Ethiopia, The land was continuously exploited and the area has been altered and modified owing to anthropogenic and many other human activities, As a result, land usage and land cover have changed, the climate has changed, and average temperature and rainfall have increased and decreased, respectively. This research identified population increase as the primary cause of ecological disruption.

In addition to the anthropogenic factors, LULC changes have been influenced by natural variables such as climate change and variability (Mendelsohn, 2011), soil conditions, and topographical characteristics, which have also accounted for LULC changes.

2.3 Processing of land use and land cover map

Image classification is a way of extracting thematic information in remote sensing by grouping similar features according to specified criteria or extracting information based on the object's reflectance. (Jensen, 2003). To represent LULC classes, digital image classification systems combine the reflectance statistics of individual pixels. The reflectance qualities of pixels called clusters were used to group these combined pixels. Based on this information, the users determine the number of clusters to obtain and the bands to utilize, and the image classification program constructs clusters. Nowadays, two types of image classification are widely employed these are unsupervised and supervised classification.

In unsupervised classification remotely sensed images are classified based on the similarity of their pixel spectral features. Without using any ground truth data, the software identifies and organizes statistical pixels with similar features. (Lillesand, 2004).

In supervised classification, the users select a representative sample of pixels from the image, and the image processing software uses this pixel as a reference to classify all other pixels in the image. The main drawback of this method is that it necessitates prior information of the land cover categories to be identified and mapped.

In this study, the supervised classification technique was applied first, followed by unsupervised classification.

The classification is not complete unless the accuracy of the classified image is verified. It is a crucial phase in the image classification process since it represents the number of correctly categorized ground truth pixels.

From several angles, the confusion matrix was widely utilized to determine the correctness of categorized LULC. These angles are User accuracy (from map users), Producer's accuracy (from map producer), and Overall accuracy (Moran, 2004). For this study, a careful analysis of the accuracy of the classified images has been conducted using an Error matrix.

2.4 Application of remote sensing

Remote Sensing (RS) is the science and art of acquiring information about a physical thing through the analysis of data obtained by a device that is not in contact with the physical object to be researched (Lillesand, Kiefer, & Chipman, 2004). For the study of historical changes in LULC, remote sensing techniques have been widely applied around the world.

The ability of remote sensing to facilitate the study of various features of the earth's surface and the spatial relationship between features, as well as the ability to obtain information from areas that are inaccessible for ground surveys, such as mountainous areas, and to save time and effort when gathering data over a large area, makes remote sensing more advantageous than traditional ground-based methods (Ahmed, 2001).

The value of various remote sensing data from various satellites has been proved in a variety of fields such as agriculture (Gebeyehu, 2019; Acharya, Pawar & Wable, 2018), cartography (Ferrari, 2019), civil engineering (JeganathanI, et al., 2017), environmental monitoring (Melesse et al ., 2007), forestry (Wubie, 2015), drought monitoring (Berhan, 2011), water resources management (Gebre, Tesfaye, & Taye, 2015); land resources analysis and land use planning (Somvanshi, PhoolKunwar, & Singh, 2018).

Map and classify LULC changes are some of the applications of remote sensing technology in mapping and researching LULC changes (Assen, 2011), assess the spatial arrangement of LULC (Mallupattu & Reddy, 2013), allow an analysis of time-series images used to analyze landscape history (Yang & Lo, 2001), analyze LULC changes impact on soil erosion (Lemilem et al., 2017), and report and analyze results of inventories including inputs to Geographic Information System (GIS), provide a basis for model building (ALI, 2009).

The open-source satellite imagery used in this study is derived from Landsat-5, Landsat-7, and Landsat 8 images that are offered on the GEE developer catalog (https://developers.google.com/earthengine/datasets).

The analysis of the LULC change in underdeveloped nations like Ethiopia becomes quite simple due to the application and presence of remote sensing technology. DEM and land cover maps are two key spatial data sources for hydrological modeling that may be obtained using remote sensing.

2.5 LULC Change detection

Change detection is the identification of differences in two or more images of the same location taken at different times (Singh, 1989). Many change detection methods were developed and used for various applications. However, the change detection techniques can be broadly divided into two approaches these approaches are Pre - Classification and Post-Classification.

In the pre-classification approach, the image values are not categorized for the change analysis The most common and widely used pre-classification approach is Vegetation Index Differencing (NDVI) (Zaitunah et al., 2018), normalized difference water index (NDWI) (Serrano, Shahidian, & Silva, 2019), Change Vector Analysis (CVA) (Xiaolu & Bo, 2011; Dewi, Bijker, & Stein, 2017), etc. They are simple, effective at detecting and locating change, and simple to execute. However, three components of pre-classification techniques are critical: picking a good vegetation index to identify altered areas, and they cannot offer specifics about the kind of change or provide a matrix of change information.

The post-classification approaches separate images and assess the differences of images pixel by pixel, providing comprehensive ‘from–to' change class information that is critical for landscape monitoring. (Ernani & Gabriels, 2006).

In general, choosing an appropriate approach to detecting change is critical because no single method can be used effectively for all research topics. The result of change detection from imagery can be affected by several factors, such as; the quality of image registration between multi-temporal images (Tingting Dan, 2018; Luigi Barazzetti, 2014), change detection methods, and lack of knowledge about approaches as well as analyst’s skill and experience (Shivangi Mishra, 2017), data sets availability and quality (Ayele, 2016), image pre-processing (Khorram et al ., 2013), the atmospheric conditions and shadow present in the

images (Gustav Tolt, 2011), acquisition times of the image (Khorram et al., 2013) and landscape and topography characteristics of the study areas.

2.6 Land - cover and land-use change in Ethiopia

Various studies have been undertaken in diverse locations of Ethiopia using various approaches and methods for studying LULC changes. For instance**,** (Asitatikie, 2019) investigated how LULC change affects the hydrology of the Rib catchment, Lake Tana sub-basin. The study discovered a 29.94% increase in cultivated land and a 6.143m3/s increase in streamflow.

Fentie et al., (2020) did another investigation to investigate LULC variations and their cumulative effects on the chemical and physical qualities of soils within the Tejibara watershed over 30 years (from 1989 to 2019). In this study, the amount of forest and grazing land has decreased, creating changes in soil attributes. As a result, the land has been degraded, and the soil's productivity has decreased.

Dinka & Chaka, (2019) conducted similar research on the Adi watershed in Ethiopia's central highlands. Significant LULC cover changes have occurred in this watershed, particularly the conversion of natural cover to managed agro systems. Furthermore, the report stated that farmland has been rapidly expanded, resulting in a decrease in plant diversity and the emergence of deforestation as a result of this expansion.

In a study conducted by Aneseyee et al., (2019), The amount of erosion and sediment supplied from the Winike watershed, Omo Gibe Basin, as a result of the LULC cover shift was estimated. The study discovered that cultivated land suffers from excessive sediment loss and erosion, as well as a decline in vegetation cover. The high association between soil loss and sediment delivery with the growth of farmed land is measured statically by the researcher.

Another study was conducted by Kinati et al., (2018 on the Didessa river basin, southwest Blue Nile, to analyze the effect of LULC change on river flow and soil erosion. The study has determined grassland, shrubland, and forest were the major LULC class that has been changed to cropland because of population increase.

Results of this study show that the LULC change that occurred during the study period resulted in an increment of average sediment yield by 20.9 t ha^{-1} yr^{-1}.

Negese, (2021) performed a comprehensive review of different studies done so far in Ethiopia on the impacts of LULC change on soil erosion and hydrological responses. In his review, he found that due to the changing of LULC the rate of soil erosion and the hydrological imbalance increased and altered significantly in the country. He also noticed that among the available LULC types the features like forest land, shrubland, grassland, and cultivated (agricultural) land had been expanded more. Finally, the researcher concluded that the major cause of this change in Ethiopia is a human-induced problem for a different purpose, especially for agricultural needs.

Overall, global LULC change is accelerating, particularly in developing countries like Ethiopia. It has a wide range of consequences, from climate change to biodiversity loss. As a result, it's critical to assess the shifting trend and its implications in Ethiopia as a whole, as well as in the kulfo catchment in particular.

2.7 Google Earth Engine

GEE is a powerful cloud-computing platform that provides the whole Landsat collection and allows for rapid scientific analysis and export (Navarro, 2017). It allows scientists, researchers, and developers to visualize a large geographical dataset using advanced machine learning algorithms. Massive satellite images can be directly obtained from this platform, and image processing can be evaluated and executed using machine learning algorithms (Tsai, 2018; Midekisa, 2017).

GEE Explorer and Code Editor are two web-based platforms that are currently available to anyone who has registered to use them (Gorelick et al., 2017). GEE has been used in a variety of studies because it is a new application. GEE contains a wealth of data from satellites, ranging from the Landsat program to a variety of climatic datasets.

GEE has been used in a variety of applications. These will be used to analyze LULC change and provide a suitable foundation for additional investigation on a separate platform(Wahap & Shafri, 2020). Its capability in detecting space-time land cover change

(Sidhu, Pebesma, & Câmara, 2018). GEE is frequently used to investigate the Spatio-temporal distribution of drought conditions and to determine the severity of drought.

The applications of GEE is very wide-ranging from drought assessment (Sazib & Bolten, 2018), mining, agriculture and ecosystem services (Goldblatt et al., 2017), drought monitoring, vegetation mapping, and monitoring (Poortinga, et al., 2018; Tsai, et al., 2018), mapping of cropland extent (Xiong et al., 2017; Prasad et al., 2017), historical

LULC mapping (Geetha, Ashagowda, & Sudhira, 2019) up to disaster management and earth sciences (Sproles et al., 2018; Liu et al., 2018; Mateo et al, 2018; Lobo et al., 2018).

Overall, all studies agree that GEE is capable of creating multi-temporal maps or conducting time series analysis using the available satellite images in the platform, fast in terms of time and processing multiple datasets quickly and efficiently with minimal human interaction, and analyzing a wide variety of data simultaneously in one consolidated system. The GEE platform could be a very useful and quick tool for analyzing satellite images and doing remote sensing analysis of large andlong-term data.

The GEE have various advantages the major benefit of it is that the data is preprocessed and ready to use, and a large number of processed and unprocessed data can be maintained effortlessly(Gorelick, et al., 2017). Because the GEE's easily accessible and user-friendly properties provide a convenient environment for interactive data and algorithm development, users may contribute and construct their data and collections using Google's cloud resources to execute all of the processing. (mutanga & kumar, 2019).

The main limitation of the GEE platform is its dependence on an internet connection and in filtering the cloud cover. In the wet season, it is very difficult to get an image that is free from cloud cover using the cloud cover masking function available on GEE. For instance, in this study for the year 2020, the cloud cover threshold has been selected as less than 1% but still, there was a cloud cover at the most upper part of the catchment.

2.7.1 Machine Learning Classifiers in GEE

Machine learning algorithms organize and classify pixels based on inputs (imagery and training data). Since the algorithm is a "black box," the researcher may inspect the inputs and outputs. GEE has a number of machine learning classifiers that may be used for both supervised and unsupervised classification. Random forest, support vector machine, decision tree, Naive Bayes, nearest neighbor, and other supervised algorithms are common(Ayodele, 2010).

In this study, land cover classification of the multispectral image is investigated using four different machine learning algorithms that achieve an appropriate result for LULC, and their accuracies are compared.

2.7.1.1 Support Vector Machine (SVM)

Support vector machine (SVM) is a non-parametric machine learning classifier that is available in Google Earth Engine (Lin et al., 2015). As first proposed by Vapnik, (1999)

it is a classification algorithm based on statistical learning theory that is theoretically capable of catching crucial spectral signatures with only a few training samples (support vectors) deriving the hyperplane to achieve reliable and satisfied land cover classification. The classification problem in support vector machines is tackled by determining the optimal interval between distinct classes by finding the best hyperplane of the feature space (Haykin, 2008).

The hyper line of SVM is described on Vapnik, (1999) by the following equation:-

$$y_i(w_i + b) \geq 0 \ldots\ldots\ldots\ldots\ldots\ldots\ldots\ldots\ldots\ldots\ldots\ldots eq(2.1)$$

Where: - xi is the point lying on the boundary of the hyperplane, w is the weight vector, and b is called the bias.

Finally, (Haykin, 2008) concluded that "SVM classifier provides an analytic approach for determining the optimum size of the feature (hidden) space, thereby assuring optimality of the classification task". Peng Fang et al., (2020); Rudrapal & Subhedar, (2015), described the performance of SVM it performs well in small and multi–future data sets.

Many studies have demonstrated the capability of SVM in land cover mapping and suggest it would be an effective algorithm for deriving the changes of land cover using 30- meter resolution Landsat images. For example, a study conducted in Malaysia, Klang Valley, used an SVM classifier to classify satellite remotely sensed multispectral data. The study emphasized that SVM classified the land covers within the study area with high accuracy (Bahari, Ahmad, & Aboobaider, 2014).

A similar study in Mongolia effectively applied SVM for mapping the historical land use land cover change as a result of the changing trend and types of features changed. The mapping has been successfully done with the best performance capability of the SVM classifier, and the overall accuracy was very high (Jamsran et al., 2019).

Shi & Yang, (2015), demonstrate the effectiveness of SVM for heterogeneous land cover mapping, the study found that SVM can significantly improve mapping accuracy, particularly for spectrally and spatially complex land cover categories. In addition to the mapping of LULC, SVM has been used for various purposes for example in groundwater potential mapping (Naghibi, 2017), modeling low flow time series (Sahoo, 2019), and groundwater quality evaluation (Lin, JunMin, & XiaoXue, 2010).

All of the studies have found that SVM had strengths in terms of classification accuracy and training time. As a limitation, the studies suggested that the classification accuracy of SVM can be affected by the size and quality of the training sample.

2.7.1.2 Classification and Regression Trees (CART) Classifier

CART is a sophisticated technique that uses a decision tree (DT) classification algorithm to build a decision tree from a collection of training data. The choice is made based on the attribute with the largest normalized information gain(Breiman et al., 1984).

CART's ability to handle both numerical and categorical data makes it easier to comprehend, visualize, and interpret the classified images (Ray, 2019). Additionally, it differentiates the most significant variables from non-significant ones (Shelestov, 2017; Bittencourt & Clarke, 2003).

The CART classification algorithm repeatedly splits input data based on a statistical test to increase the similarity of the training data in the resulting node (Mondal et al., 2019). The main limitation of the CART algorithm is the presence of high variance across samples this leads to occupancy of high variability in predicting classes and estimates (Hayes et al., 2015)

2.7.1.3 Random Forest (RF)

A random forest classifier uses training data to identify statistical patterns in huge datasets and then selects the best classification for all pixels within imagery using a succession of decision trees(Breiman, 2001). It's a nonparametric machine learning technique that uses multiple decision trees to categorize a random sample of training data using covariate predictors. The majority vote among all trees determines the final class and model development options (Breiman,2001).

Because the effectiveness of a random forest classifier is not affected by the number of variables per split, the user can define the number of trees and variables per split in a random forest (Breiman et al., 1984).

The Random forest method has several advantages such as more efficient results for large data (Herrera et al., 2019; Zakariah, 2014), can handle thousands of variables without reducing it (Rodriguez et al., 2012), gives an estimate of variables that are important in classification (Robin Genuer et al., 2010; Frauke Degenhardt et al., 2019), can produce unbiased estimates of generalization errors (Siroky, 2009) and computationally lighter than other tree ensemble methods.

Many studies have demonstrated the effectiveness of using the random forest classifier in LULC mapping. For example, Nurfadila et al., (2019) used Sentinel 2 satellite data with a spatial resolution of 10 m to map land use and land cover change, resulting in more optimal LULC maps with a 95% overall accuracy. Moreover, this classifier has been used widely to classify satellite data for wetland mapping (Masoud et al., 2017; Shaohong et al., 2016), cropland mapping (Oliphant, et al., 2019) , and natural hazard susceptibility area mapping (Taalab, Cheng, & Zhang, 2018; Sunmin et al., 2017).

2.7.1.4 Naïve Bayes

The Bayesian theory of probability and predictions of the unknown class are used or applied by a naive Bayes classifier, which assumes that the features have substantial (nave) independence. This makes the nave Bayes classifier a probabilistic model (Camargo et al., 2019).NB assumes that the feature class doesn't depend on the presence and absence of any other feature class instead it depends on the nature of the probability model this makes the datasets train quicker (Ratika Pradhan, 2010).

The ability to work with a small number of training data sets, ease of use and understanding, and speedy training and classification distinguish the Naive Bayes classifier method from other types (Ho, 1998).

The NB classifier was successfully deployed for gully erosion and landslide susceptibility assessment (Chen et al., 2019), Spatial Prediction of Groundwater Potentiality, Assessing the spatial likelihood of flood hazard (Liu R. C., 2016).

2.8. Hydrological Models

Hydrological models are characterizations of the real-world system. The best model is one that produces outcomes that are as close to reality as possible while using the fewest number of parameters and having the least degree of model complexity (Gayathri et al.,2015).

Different researchers employed a variety of hydrological models, but the applications of those models are largely reliant on the goals for which the modeling is done.

2.8.1. Model selection criteria

The choice of a model is critical for achieving a satisfying outcome for a given situation, and it is made based on the problem's objectives formulated, data availability, the hydrological aspects being represented, and model simplicity(Vaze et al., 2011).

Dhami and Pandey, (2019) also stated that the essential criteria that must be answered before selecting any hydrologic models are hydrological processes, governing equations, minimum data necessary, spatial and temporal scale of the model.

There are many hydrological models developed to facilitate the simulation of water movement in watersheds until it forms stream flow this classification is generally based on the method of representation of the hydrological cycle or a component of the hydrologic cycle (Gayathri et al., 2015).

Hydrological models can be categorized into the following broad classes this is lumped or distributed, deterministic or stochastic, and conceptual and physically based models (Beven, 2000; Beven, 1985).

In lumped models, there is no spatial variability of the hydrologic parameters within the basin. Therefore, the response of the basin is evaluated only at the outlet without accounting for the detailed response of individual sub-basins (Cunderlik, 2003).

According to Cunderlik, (2003) distributed models require large amounts of data parameterization in each grid cell. He stated that distributed models can provide the highest degree of accuracy if input data are adequate and governing physical processes are modeled in detail and properly applied.

In distributed physically-based models streamflow simulation is based on complex mathematical equations. In semi-distributed models, the spatial variability of the model parameters is allowed by dividing the basin into several smaller sub-basins. The semi-distributed models are more physical based when compared to lumped models, and that they require fewer input data than fully distributed models (Cunderlik, 2003).

Deterministic models permit only one outcome from a simulation with one set of inputs and parameter values while stochastic models allow for some randomness or uncertainty in the possible outcomes due to uncertainty in input variables, boundary conditions, or model parameters (Beven, 2000).

Conceptual models are based on a limited representation of the physical processes acting to produce the hydrological outputs, while physically based models are based more solidly on an understanding of the relevant physical processes.

Now a day there are so many comprehensive spatially distributed hydrologic models have been developed in the past decade due to advances in hydrologic sciences, Geographical Information systems (GIS), and remote sensing.

Every hydrologic model, because of its special structure and basic assumptions, is developed for specific time and spatial scales. For example, The SHE (Systeme Hydrologique European) model is a fully distributed grid, element-based model. The model can predict infiltration excess runoff, saturation excess runoff, groundwater flow, and subsurface contribution to the hydrograph but the application of the SHE model requires thousands of effective parameter values at the grid element scale (Abbot et al., (1986a, 1986)).

According to Nourani et al., (2011) HEC-HMS and unit hydrograph methods are not able to estimate exactly the amount of water content in the soil column, especially before and after long periods because these models are event-based and cannot be appropriately applied for long-term stream and sediment yield modeling.

SWAT (Soil and Water Assessment Tool) is a deterministic, continuous watershed model that may operate on daily and hourly time increments and is available in the public domain graphical user interface program (Addis, 2016).

The model was created at the Grassland, Soil, and Water Research Laboratory in Temple, Texas, by the US Department of Agriculture – Agriculture Research Service (USDA-ARS) (Arnold J. G., 1989). It models hydrological processes, sediment yield, nutrient loss, pesticide losses into surface and groundwater, as well as the effects of agricultural management techniques on the water in vast watersheds (Arnold J. G., 2012).

It has been widely used by researchers throughout the world because of its ability to simulate the characteristics of a watershed using various scenarios. (Blainski et al.,2016), allows considerable spatial detail for basin-scale modeling (Heuvelmans, 2004), and users readily available inputs for weather, soil, land, and topography.

2.8.2 Hydrological component of SWAT

SWAT allows modeling a variety of physical processes in a watershed. The simulation of a watershed's hydrology is done in two separate components. These are the land phase and the routing phase of the hydrologic cycle, respectively (Neitsch et al, 2011). The hydrologic cycle's land phase regulates water movement on land and dictates the amount of water, sediment, nutrients, and pesticides that will enter the mainstream. The land phase of the hydrological cycle simulates canopy storage, infiltration, redistribution, and

evapotranspiration, as well as lateral subsurface flow, surface runoff, ponds, and tributary channel return flow. A watershed can be divided into several sub-watersheds or sub-basins for modeling purposes.

In the land phase of the hydrologic cycle, SWAT simulates the hydrological cycle based on the water balance equation (Neitsch et al, 2011) and computed by:

$$S_{wt} = S_{wo} + \sum_{i=1}^{t} (R_{day} + Q_{sur} - E_a - W_{sep} - Q_{gw}) \ldots\ldots\ldots\ldots\ldots\ldots\ldots . Eq(2.2)$$

where: - S_{Wt} is the final soil water content (mm), S_{wo} is the initial soil water content for day is (mm), t is the days (days), R_{day} is the day precipitation (mm), Q_{surf} is the surface runoff (mm), Ea is the evapotranspiration (mm), Wsep is the seepage from the bottom soil layer (mm) and Q gw is the groundwater flow on the day I (mm).

When the rate of precipitation exceeds the rate of infiltration, surface runoff occurs. Surface runoff is calculated in the SWAT model using either the SCS curve number process (USDA-SCS, 1972) or the green and Ampt infiltration method. (Green and Ampt, 1911). The SCS curve number method calculates runoff using the following Equation using daily or sub-daily rainfall for each HRUs.

$$Q_{surf} = \frac{(R_{day} - 0.2S)^2}{R_{day} + 0.8S} \ldots\ldots\ldots\ldots\ldots\ldots\ldots\ldots eq(2.3)$$

Where: - Q_{surf} is the accumulated runoff or rainfall excess (mm), R_{day} is the rainfall depth for the day (mm), S is the retention parameter (mm).

The retention parameter is defined by equation 2.4

$$S = 25.4 * \frac{1000}{CN} - 10 \ldots\ldots\ldots\ldots\ldots\ldots\ldots\ldots\ldots\ldots\ldots\ldots . . eq(2.4)$$

Where: - CN is the curve number for the day and it is a function of land use, soil permeability, and antecedent soil water condition.

SWAT uses a modified rational method to compute the peak runoff rate. Many methods for estimating potential evapotranspiration have been developed (PET). Three methods are incorporated into SWAT which are the penman-Monteith method (Monteith, 1965) , the Priestley-Taylor method (Priestley & Taylor, 1972), and the Hargreaves method (Hargreaves, 1985).

These methods have a wide range of data requirements for climate variables. Solar radiation, air temperature, relative humidity, and wind speed are required for the Penman-Monteith technique; solar radiation, air temperature, and relative humidity are required for the Priestley-Taylor method; and air temperature is required for the Hargreaves method. The Penman-Monteith approach was chosen based on the data available in the catchment.

The second hydrological component simulation of the watershed is the flow routing phase, in which the water is routed in the channels network of the watershed, carrying the sediment, nutrients, and pesticides to the outlet. In the calculation of the water balance in the channel flow, the rate and velocity of flow are calculated by using manning's equation, and the transmission and evaporation are also well considered by the model. The Storage routing is based on the continuity equation

$$\Delta V_{stored} = V_{in} - V_{out} \ldots\ldots\ldots\ldots\ldots\ldots\ldots..eq(2.5)$$

where:- ΔS_{stored} Is the change in volume of storage during the time step (m3), V_{in} Is the volume of inflow during the time step (m3), and V_{out} Is the volume of outflow during the time step (m^3).

2.9 Application of SWAT model in Ethiopia

Bharti et al., (2020) used the SWAT model to analyze sediment yield in the Rib watershed and found that it provided acceptable hydrological performance. The calibrated model also provides information for using the model in other ungauged watersheds with similar topography, land use, soil, and climate for erosion assessment and implementation of best management scenarios in Ethiopia.

The superiority of SWAT model performance was also assessed by Assfaw, (2019) in performing the trend of runoff and sediment yield in Megech Reservoir, Ethiopia. Additionally, Hailu Kendie Addis et al., (2016) modeled streamflow and sediment yield in Ethiopian highlands using the SWAT model, and the performance of the model was satisfactory.

The best performance capability of the SWAT model in simulating and predicting sediment yields from the Fincha watershed and hence can be used as a tool for water resources planning and management in the studying watershed has been done and suggested by (Ayana, Chemeda, & Ekasit, 2012).

The ability of SWAT to adequately simulate stream flows was also assessed by Sime et al ., (2020) in Toba sub-watershed, Ethiopia. The daily and monthly stream flows simulation, as well as modeling of the hydrological water balance in Lake Tana Basin, was successfully investigated by (Setegn et al., 2008). Betrie et al., (2011), applied the SWAT model to simulate daily sediment yield From the Upper Blue Nile basin under different Best Management Practice (BMP) scenarios on sediment reductions, as a result, good agreement between the observed and simulated daily sediment concentrations as the value of Nash-Sutcliffe efficiency was 0.83 obtained. Similarly, Temesgen Gashaw, (2021) evaluated Best Management Practices On Soil Erosion Reduction Using the SWAT Model for Gumara Watershed, Abbay (Upper Blue Nile), and the application of the combined Scenarios such as SSB & GW, and GW & RC reduces the high soil erosion in the Gumera watershed, and similar agro-ecological watersheds in Ethiopia and many other researchers in Ethiopia has been successfully calibrated and validated SWAT model.

Therefore, SWAT can be utilized very well for hydrological simulations and able to fairly explain the hydrological characteristics in the selected catchments and can be further extended to similar watersheds in the country, particularly in the kulfo watershed of Ethiopia.

3 MATERIALS AND METHODS

3.1. Description of Study Area

The Kulfo catchment is located in the Southern Ethiopian Rift Valley's Abaya-Chamo sub-basin and flows to Lake Chamo. Kulfo's catchment area is approximately 362km2 and is located near the town of Arba Minch, stretching between 5°55'N and 6°15'N latitude and 37°18'E and 37°36'E longitude, with a total length of 23km along the channel (Figure 3.1).

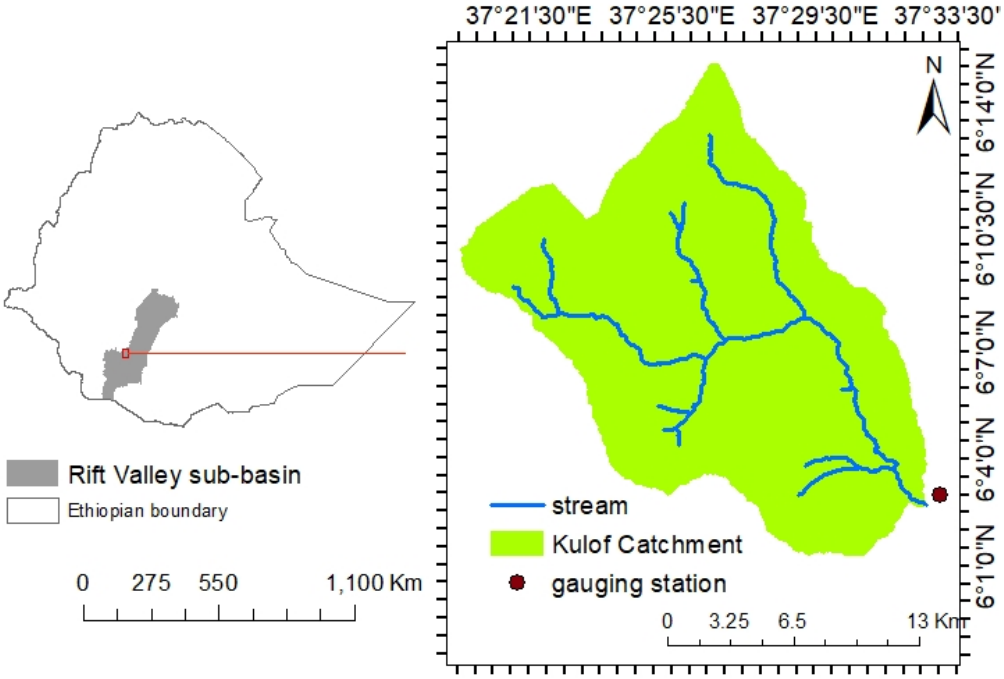

Figure 3.1 Location of the study area (Kulof Catchment)

3.1.1 Topography

The terrain characteristics of the study area were analyzed by using GIS as a result the study area was mountainous in the mid and upstream parts, and also the area is characterized by remarkable elevation difference that reaches from 3370 masl at the peak of the North-West to 1586 masl north-east and about 1227m above mean sea level at the termination to the lake Chamo (Figure 3.2 A).

The sloping terrain was classified based on the Food and agriculture organization (FAO, 1985) classification system (Figure 3.2B). About (45%) of the Kulfo catchment is classified as a steep slope and 23.5% of the terrain area is classified as very steep and 11.5% of the area is a moderately steep slope. Around 10.6% and 5.8% of the area are characterized under sloping and gentle sloping. Only 1.5% of the area was an extremely steep slope and 2.33% of the lower catchment of the river is flat.

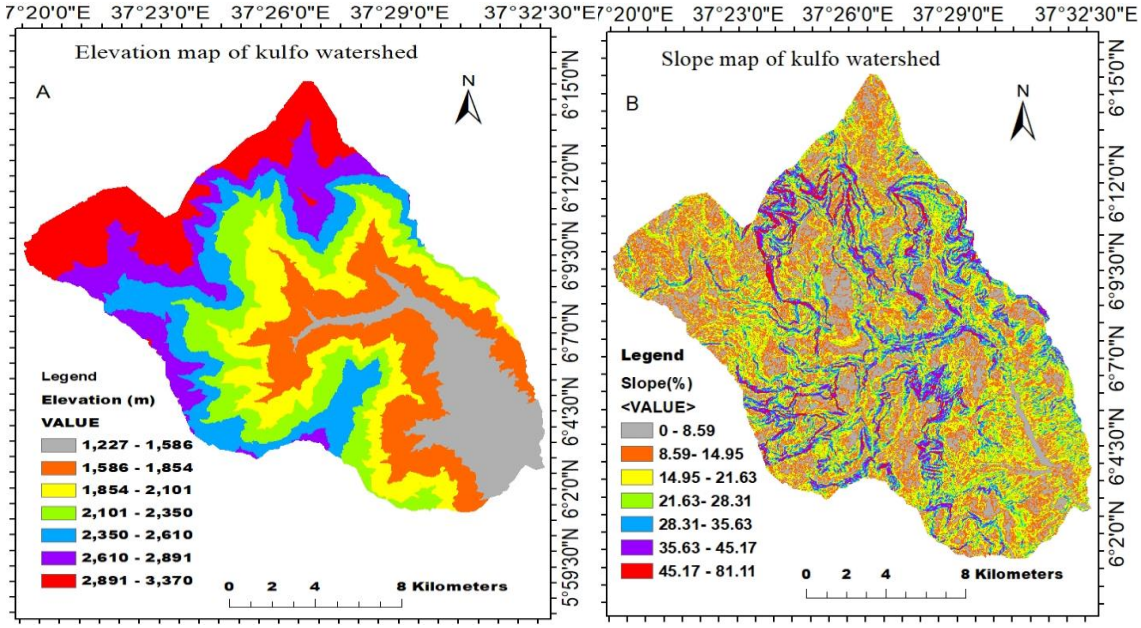

Figure 3.2 Study area descriptions: (A) Elevation map (B) Slope map of kulfo watershed

3.1.2 Climate of the study area

According to Ethiopian climate classification, the Kulfo catchment is characterized by hot semi-arid warm temperatures and a tropical climate. The average annual rainfall ranges from 665mm at Bilate to 1240mm at Chencha with an average maximum temperature of 31.2ºC at Arbaminch and a minimum average temperature of 13.9ºC at Chench (Abyot, 2008).

Figure 3.3 shows the average monthly rainfall of stations in and around the kulfo catchment. The average monthly rainfall is very high in April and May whereas it is very low from December to March.

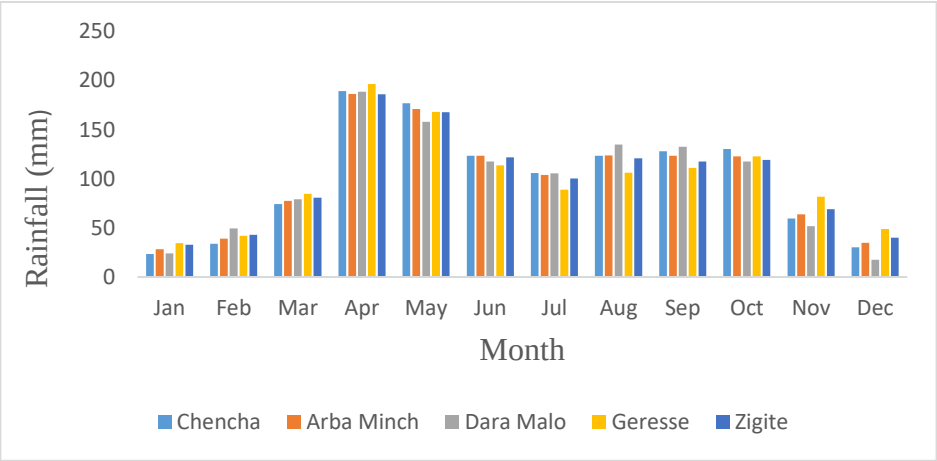

Figure 3.3 Mean monthly rainfall of stations in and around the Kulfo catchment.

3.1.3 Soil

The soil map produced in (Figure 3.4) shows that the catchment area is characterized by two major types of soil: Loam and Clay Loam. The most dominant soil texture is Clay loam, which covers about 65% of the catchment.

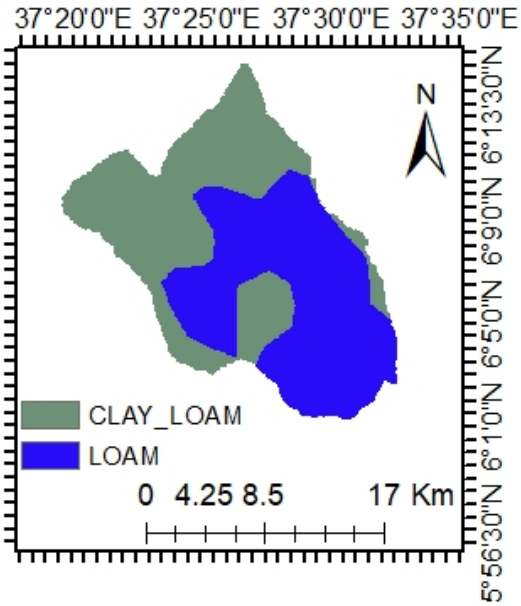

Figure 3. 4 Major Soil map of kulfo catchment

3.2 Data collection and methods

The impact of land use and land cover on streamflow on kulfo catchment has been evaluated using the SWAT model. For the completion of this study extensive fieldwork and secondary data were combined to prepare a historical LULC map.

In modeling a given watershed the quality and quantity of data, used, have a great influence on the performance of the model. Particularly, the SWAT (Soil and Water Assessment Tool) requires good quality of digital elevation model (DEM), Soil and land use, and land cover data above all other necessary data. For this study, various necessary data were collected from different sources, primary and secondary data, and used. As primary data GCS collected from each of the pre-defined land use land cover types have been collected and to get full information about the past events, human intervention activities, and the previous land use land cover types, information's had been gathered from the local community. The secondary data used were DEM data, soil data, land use/land cover data, flow, and climatic data. Generally, the data are mainly classified into two main categories they are spatial and time-series data. The types, quality, and quantity of data used in the development of the SWAT project in this study have been discussed in the next sections.

3.2.1 Field Data

Before visiting and going to the field the major land use land cover class were determined (identified) using an unsupervised classification method. Then several field visits, aided using GPS, were carried out to collect ground control points (GCPs). An informal interview was conducted to obtain additional information about the past LULC in the catchment. The main methods followed for the discussion and in-depth interview were interviewing selected peoples personally as well as preparing group discussion with the local communities for this systematic approaches were followed like a selection of elder peoples and landowners, making the number of interviewees more on the controversial area. About 50 selected elder and local communities were asked from different Kebele and areas of the catchment.

The major purpose of the field survey was to determine the major land use land cover class in the study area and for accuracy assessment.

A minimum of 40 and a maximum of 50 ground control points had been collected from the field from each of the classified land use and land cover classes. During the collection of GPS points, very high attention was given to the major key features that existed within the watershed since it helps more for georeferencing of classified images.

3.2.2. Spatial data

A digital elevation model (DEM) is an important spatial input for the automatic extraction of topographic parameters for the soil and water assessment tool (SWAT). Topography is defined by a DEM that describes the elevation of any point in a given area at a specific spatial resolution. The watershed characteristic like a length of the streamline, the main channel slope, the watershed area, the area slope varies for different types of DEM resolution (Waranyu, 2016).

So, DEM data has a significant effect on the hydrological modeling of a watershed. Therefore, in this study, the DEM (Digital Elevation Model) data with (30mx30m) resolution in raster format was used and projected to Transverse Mercator (UTM) on the spheroidal of WGS84 to correct the errors and fit into the model requirements. It was obtained from the ministry of water irrigation and electricity (MoWIE), GIS Department. Figure 3.5 shows the digital elevation model (DEM) of the kulfo watershed.

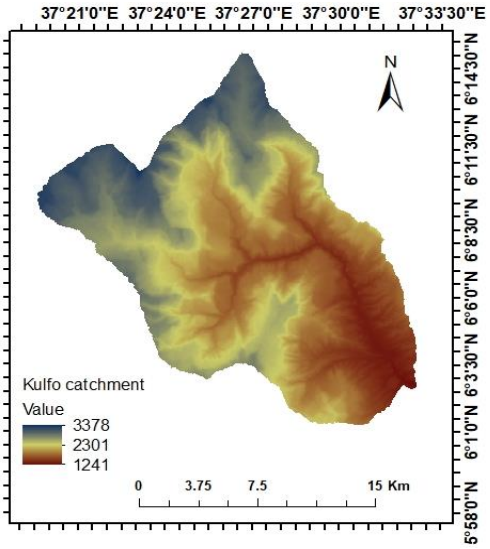

Figure 3.5 Digital Elevation model of Kulfo catchment

The second very important type of data used was land use and land cover which greatly affects the hydrological response of a watershed and defines the densities and types of land use found within a given area as well as determines the watershed characteristics. Therefore, detailed analysis and mapping of the land use/land cover is crucial for proper hydrological modeling

This study used the Google earth engine platform to analyze and map land use and land cover change from 1986-2020, as a result, the dominant land use type in 1986 was shrub land which covers 108.34 km^2 followed by agricultural land then after more than a decade in 2000 the catchment was dominated by agricultural land that occupies 34.49% of areal coverage whereas in 2016 the agricultural land increased and covers 47.95% of areal coverage and the recent year 2020, was dominated by agricultural land with areal coverage of 57.12% Table (4.3).

Soil data of the catchment was obtained from the ministry of water irrigation and electricity (MoWIE), GIS section. The determination of the available dominant soil types on the study area was analyzed by using ArcGis 10.4 software as result the dominant soil types are Clay-Loam, and Loam.

Table 3.1 dominant Soil types of kulfo catchment

Soil Group Name	SNAME	Soil Group	Area (km2)
Clay Loam	CM	D	165.1
Loam	NT	C	157.704

3.2.3 Time series data

To simulate the hydrological condition of the catchment SWAT model needs hydrological and metrological data sets. The main metrological data sets used were daily data of precipitation, maximum and minimum temperature, relative humidity, wind speed, solar radiation, and sunshine hour which were obtained from the National Meteorological Services Agency (NMA) of Ethiopia with a different record length of the year.

Table 3.2 Summary of rainfall and stream gauging stations

S.NO	Station/Site	Latitude	Longitude	Elevation	Record length
1	Arba Minch	6.05	37.549	1652.59	1987-2004
2	Dara Malo	7.06	38.47	2005	1991-2003
3	Geresse	14.2	39.4	2506	1992-2002
4	Zigite	6.319	37.23	1914.25	1992-2005
5	Chencha	6.23	38.01	1813.36	1992-2004

For performing sensitivity analysis, calibration, and validation of the model, streamflow was required. Hydrological data like an observed daily flow which covers a period of 1991 to 2004 years was collected from the Ministry of Water, Irrigation and Electricity with some missed value for Arba Minch hydrological stations.

3.3 Data analysis and Quality checking

3.3.1 Filling of missed data

Some precipitation stations may have short breaks in the records because of the absence of the observer or because of instrumental failures thus filling in missed data is very vital to perform hydro-meteorology analysis and simulation using data of long time series.

There are methods to fill in missing data. These are: arithmetic mean method, normal ratio method, and inverse distance weighting method.

When normal annual precipitation is within 10% of the gauge/station for which data are being reconstructed, the arithmetic mean method can be used to fill in missing data. When the normal annual precipitation at any of the index stations differs by more than 10% from that of the precipitation station, the normal ratio approach is applied. In the absence of the stations' normal annual rainfall, the inverse distance weighting approach can be employed to fill in the gaps.

In this research, the arithmetic mean of the entire period was used to fill the missed records for the stations with less than 10 percent missed records and by using Microsoft excel the regression formula is used to calculate the missing data of stations before the data is used by the model.

3.3.2 Consistency of Rainfall Data

Time-series data is consistent when the characteristics of the record have not altered throughout time. Some of the most prevalent causes of the inconsistency of records are shifting of rain gauge station to a new location, the neighborhood of the station undergoing a marked change, change of ecosystem due to climates, and occurrence of observational error from a certain date.

The method of double mass curve analysis is used to determine if rainfall data obtained at a certain rain gauge station is consistent or inconsistent. The method for checking the consistency of meteorological data using double mass curve analysis is determined by plotting the cumulative values of observed time series of the station for which consistency needs to be checked on one axis versus the cumulative value of observed time series of a group of stations on the other axis and the station affected by the trend.

The data series, which is inconsistent, adjusted to consistent values by proportionality.

$$S_i = \frac{\Delta Y}{\Delta X} \ldots\ldots\ldots\ldots\ldots\ldots\ldots\ldots\ldots\ldots\ldots .3.1$$

where:- S_i – the slope of section I, ΔY – the change in the cumulative for gage Y between the end points of section I, ΔX – the change cumulative for the sum of the regional gage between the endpoints of section i.

$$P_{cx} = P_x * \frac{M_c}{M_a} \ldots\ldots\ldots\ldots\ldots\ldots\ldots\ldots\ldots\ldots\ldots\ldots\ldots\ldots\ldots .3.2$$

where:- P_{cx} is corrected precipitation at any period, P_x is Original recorded precipitation at any period, M_c is corrected slope of double mass curve, M_a is the original slope of the double mass curve.

The following graphical sketch of the double mass curve as seen in Figure 3.6, shows relative consistency of the selected stations, with no slope variation in between the time series data of all rainfall stations, So that the correction of consistency was not been done.

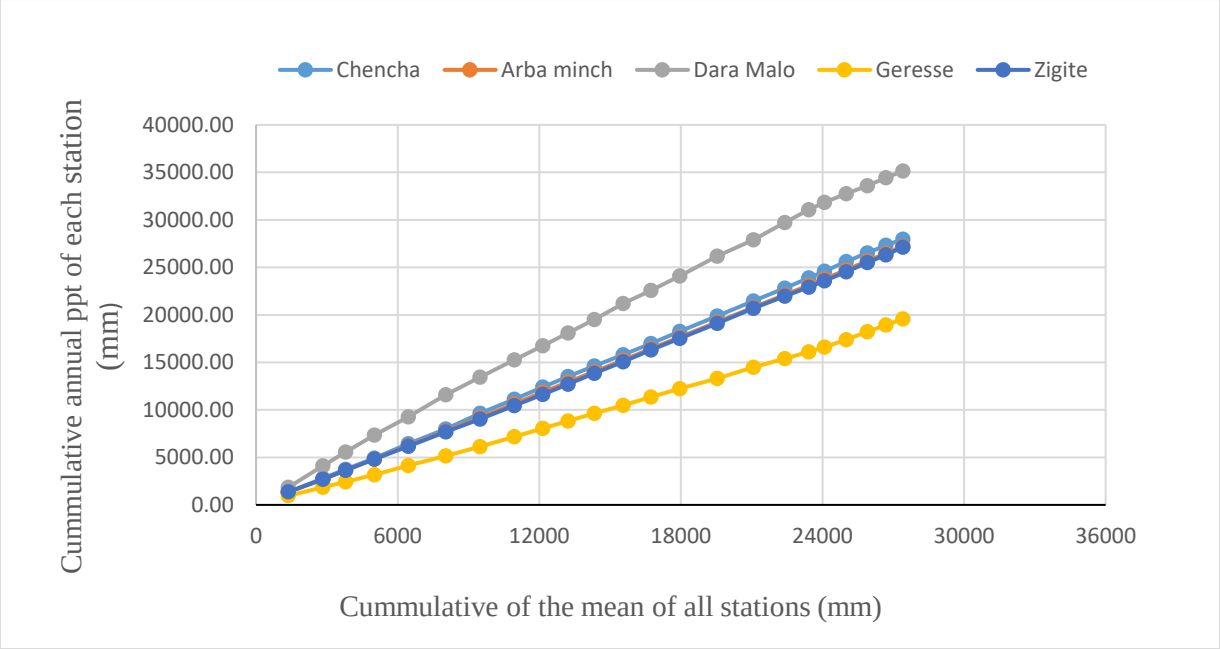

Figure 3.6 Test for consistency of rainfall station by DMC method

3.3.3 Homogeneity and trend test

Graphical comparison of the rainfall data done by creating time-series plotting of monthly percentage of rainfall data (see figure.7) showed that the four stations show a similar periodic pattern of records. Because of the uncertainty about possible changes, graphical methods are often used in climatology and hydrology to obtain some insight into the homogeneity of a record. The plotted points tend to fall along a straight line under conditions of homogeneity. In this study homogeneity is an important issue to indicate the trend of the rainfall data. One of the methods to check homogeneity of the selected stations in the watershed is the non-dimensional rainfall records and plotted to compare the stations with each other and the line of best fit was sketched.

$$P_i = \frac{P_{i,avg}}{P_{avg}} * 100 \ldots\ldots\ldots\ldots\ldots\ldots\ldots\ldots\ldots\ldots\ldots\ldots eq(3.3)$$

Where: - P_i – is the non-dimensional value of precipitation for the month in the station I, $P_{i,avg}$ – is over years averaged monthly precipitation for the station I, P_{avg} – is over years averaged yearly precipitation of the station.

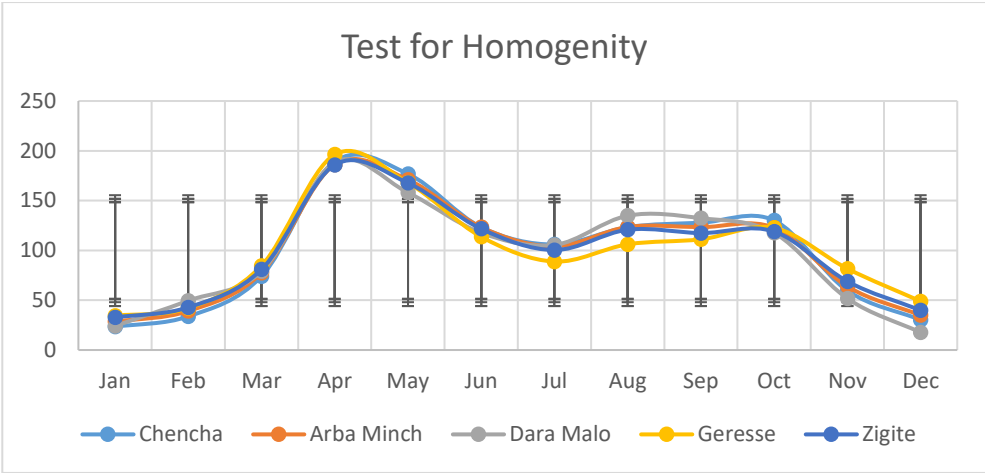

Figure 3.7 Homogeneity Test for rainfall stations

The percentage of rainfall of each station was drawn on the y-axis and the months were drawn on the x-axis to check the homogeneity of each rainfall station. When the rainfall patterns are spatially identical or vary within a range, they could have been considered homogeneous. The above graphs showed all points set on or form almost the same pattern, which was plotted for checking of homogeneity of rainfall pattern, all stations were consistent and have acceptable homogeneity. The same rainfall trend and with high rainfall season in April and May.

3.3.4 Test for outliers

An outlier is an observation that deviates significantly from the bulk of the data, which may be due to errors in data collection, or recording, or natural causes. The presence of outliers in a time series data causes difficulty when fitting a distribution to the data. Low and high outliers are both possible and have different effects on the analysis.

$$X_H = exp^{(x+KNS)} \ldots\ldots\ldots\ldots\ldots\ldots\ldots\ldots\ldots\ldots\ldots\ldots\ldots\ldots eq(3.4)$$

$$X_L = exp^{(x-KNS)} \ldots\ldots\ldots\ldots\ldots\ldots\ldots\ldots\ldots\ldots\ldots\ldots\ldots\ldots eq(3.5)$$

Where X and S are the mean and standard deviation of the natural logarithms of the sample, respectively, and kN is the G-B statistic tabulated for various sample sizes and significance levels by Grubbs and Beck (1972). At the 10% significance level, the following approximation proposed by (Pilon et al., 1985), is used, Where N is the sample size.

$$KN = -3.62201 + 6.28446N^{\frac{1}{4}} - 2.49835N^{\frac{1}{2}} + 0.491436N^{\frac{3}{4}} - 0.037911 \ldots\ldots eq(3.6)$$

Sample values greater than XH are considered to be high outliers, while those less than XL are considered lower outliers. Firstly, the time-series data have been arranged using the

annual maximum model that takes only one representative value for each year in the study periods. Then using the formulas (equation 3.4 and equation 3.5) the outlier of the time series data have been checked and some values of outlier have been detected mostly in the maximum side for flow and rainfall.

3.3.5 Hydrological data analysis

For this study 13 years of flow, data was used from 1991-2004 was used for Arba Minch station only from this two-thirds for calibration (from 2003-2000) and one-third for validation (from 2001-2004) but two years for worm up period from 1991-1993 and the missing was completed by regression analysis.

3.4 Materials

Table 3.3 the materials and software tools used for this study were

No.	Materials	Version	Purpose of the material
1	ARC GIS	10.4	Preparation of and processing of data
2	Google earth engine		For land use land cover map processing and preparation
3	GPS	GARMIN	For the collection of ground truth points
4	SWAT	2012	Simulation
5	SWAT-CUP	5.1.6	Sensitivity analysis, calibration and validation
6	Weather database.	v01803	Preparation of weather generation
7	Google earth pro	7.2.3	For investigating historical images and Study area
8	MS EXCEL	2016	Statistical analysis, Chart, and graphs

3.5 Methods

The Google earth engine application, a JavaScript API, was used to analyze the spatial and temporal land use and land cover dynamics. The JavaScript API codes were taken from (https://earthengine.google.org/). However, the script was customized for the current usage (study area).

The Landsat series of satellites have provided continuous imagery for the past few decades. These images are contained in Google Earth Engine's public data archive and can be used to detect and estimate the long-term dynamic of land use land cover change.

Google Earth Engine greatly reduces the analysis time by utilizing Google's distributed computing infrastructure platform (https://earthengine.google.org/). It provides excellent performance in terms of enabling access to remote sensing products through the cloud

platform and providing pre-processing to archived data from the US Geological Survey (USGS) collection (Zurqani, et al., 2020).

This paper uses annual composites Landsat Surface Reflectance images covering an area around 362km^2 of, kulfo, the catchment for classification and further analysis. Four annual composites images from four Landsat Series were used in this study.

When selecting the right type of data set several aspects have to be considered; the most important are availability, accessibility, and quality of the data (Aitkenhead and Aalders 2011).

The satellite imagery used in this study to classify LULC changes were the Landsat Thematic Mapper (TM) of 1986, the Landsat Enhanced Thematic Mapper Plus (ETM+) of 2000, the Landsat Enhanced Thematic Mapper Plus (ETM+) of 2016, and the Landsat Operational Land Imager (OLI) of 2020 each of them was analyzed individually and change detection analysis was done by performing pre-and post-change detection techniques.

A large number of high-quality samples were selected by visual interpretation and google earth images were used for selecting training samples to improve the classification accuracy. Four popular machine-learning algorithms of SVM, CART, RF, and Naive Bayes were employed to identify and map long-term LULC change.

The Landsat archived data from the US Geological Survey (USGS) collection was loaded as an Image Collection and the selected study area was injected into the GEE and displayed.

The LULC classification technique was applied and evaluated by developing code in the GEE platform using the supervised classification method and Landsat imagery for each chosen year.

In this study, four types of Machine learning classifier algorithms, available on GEE, were applied and the best performing one was selected. This Machine learning classifier algorithms were SVM, Random Forest, Naïve Bayes, and CART. After, processing the land use and land cover map the result has been exported to google drive. All of the processing was conducted in GEE Code Editor (*https://*code.earthengine.google.com/).

3.5.1 Image pre-process in GEE

To avoid confusion and overcome timeout error four customized GEE Code Editor Scripts were used to the individual year separately (1986, 2000, 2016, and 2020). Each of the individual year images had passed the following main components of image preprocessing.

3.5.1.1 Acquiring Landsat Surface Reflectance image collection

The first step is accessing and acquiring data started by a function to call and make a composite image by calling a series of images from the Image Collections.

3.5.1.2 Image mosaicking and cloud removing

After acquiring the required image collections the next step was injecting the shapefile of the study area to google earth engine platform in the form of zipped file format and a selected year Landsat image collection is loaded by filtering the date of acquisition this is done to minimize the effect of the rainy season on the classification result. Then, a cloud-masking function was developed by assigning a cloud score to each pixel in the image collections for the removal of cloud covers, for this a cloud threshold of 1% and 5% was selected based on the visual interpretation of Landsat imagery. This cloud masking function computes a cloud-likelihood score to compare multiple views of the same point for a relative cloud likelihood, and pixels with a cloud-score higher than 1% and 5% were masked out. The filtered image collections were acquired after the cloud mask, and a limited date range was applied.

3.5.1.3 Collection of Training Data

For the collection of training data (samples) for land-cover types, the study area was clipped, and true color composite and false-color composite methods were used for the extraction of spectral and spatial features from Landsat images based on the pixel-based approach. This helps to select training points effectively for each of the land cover types.

In this study, six land use and land cover categories (Bare Land, Agricultural Land, vegetation, shrub land, and Grassland) have been detected and collected using the pixel-based approach.

To assess LULC change over time with GEE, a total of training samples ranging from 507 to 776 for the years 1986, 2000, 2016, and 2020, were selected and collected. Among these sample points, 70% were gathered as training samples during classification. The remaining points were used to verify the accuracy of the classification results.

In the distribution of training sample points moderately cultivated, croplands, farm Lands, and other types of plantation areas were classified under agricultural land cover class whereas plants like banana, avocado trees, and sugarcane which are planted around the river are grouped as a vegetable class and also areas which are moderately populated by trees and higher than shrub lands in height, as well as false banana, were reclassified under Mixed forest class.

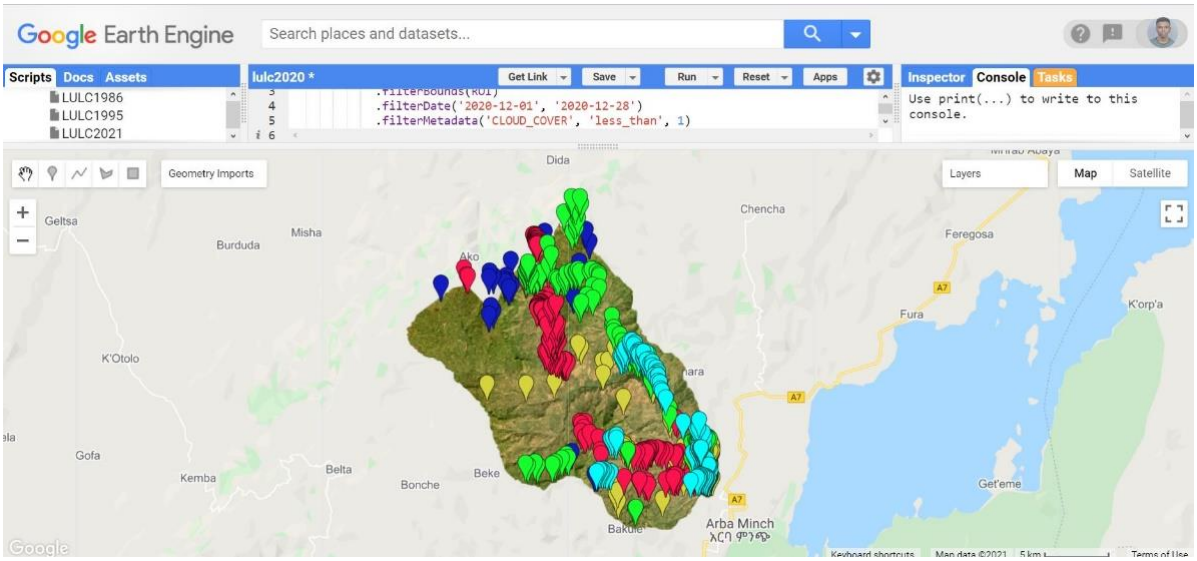

Figure 3.8 Training Data sets

3.5.1.4 Image Classification

The obtained image composites were then classified within the GEE using 4 different types of classifiers which were Support Vector Machines(SVM), Random Forest(RF), Naive Bayes, and CART algorithm with the following six land-cover categories bare land, agricultural land, vegetation, shrub land and Grassland and.

Finally, the relevant results from the analysis such as charts, images, maps, and tables from classified images were exported to google drive.

3.5.1.5 Land use land cover data Processing

The land use land cover is procced and generated by Google earth engine among the classified class of land use and land cover class the dominate one was agricultural land and the generated land use and land cover is converted to SWAT database code for running of SWAT model as shown in Table 3.4.

Table 3.4 Original and the redefined land use/land cover types of kulfo catchment

Original land use land cover	Redefined land use and land cover according to Swat database	SWAT code
Shrub land	Forest-Deciduous	FRSD
Agricultural land	Agricultural land closely grown	AGRC
Grassland	Range grasses	RNGE
Bare land	Barren	BARR
Mixed Forest	Forest mixed	FRST
Vegetation Cover	Forest-Evergreen	FRSE

3.6. SWAT Model

This study uses Arc swat 2012 to generate a hydrologic model of Streamflow from the study catchment, Kulfo, in a GIS used interface.

3.6.1 Model set up

SWAT allows a number of different physical processes to be simulated in a watershed. The simulated processes include surface runoff, infiltration, evapotranspiration (ET), lateral flow, percolation to shallow and deep aquifers, and channel routing (Neitsch, 2011; Arnold., 2012).

SWAT model passes three main preprocessing steps this are watershed delineation, hydrologic response unit (HRU) analysis, and weather data definition and SWAT model simulation part with that of sensitivity analysis, calibration, and validation. Therefore, the major steps of Arc SWAT preprocessing will be discussed in depth.

Watershed Delineation

The primary step in creating a new SWAT model project besides preparation of input data is watershed delineation from digital elevation model for this a new project set up and necessary folders as well as databases have to be created to store all the output data processed from the model.

The Watershed delineation process involves five major steps, DEM setup, stream definition, outlet definition, watershed outlets selection, and definition. After, a successful compilation of DEM setup and manual specification of the location of outlet on the DEM, the model automatically calculates the flow direction and flow accumulation as well as stream networks, sub-watersheds, and topographic parameters.

The size of the sub-basin in the watershed will affect the assumption of homogeneity. In this study, the delineation of the watershed has been done using 30m by 30m DEM resolution and the watershed outlet is manually added and selected for finalizing the watershed delineation. With this information, the model automatically delineates the watershed with 25 sub-watersheds for simulations.

Hydrological Response Unit Definition

After performing the automatic watershed delineation, the watershed was partition into hydrological response units (HRUs), lumped land areas within the sub-basin, which incorporates the same land use, soil, and management practice. Any parcels of lands within

one sub-basin that share the same combination of these three features, land use, soil, and management practice, will be considered one HRU.

SWAT has predefined land use classes in its crop database. So it is necessary to prepare a look-up table, which refers to land use land cover classes found in hand with SWAT land use land cover. So, the Grid code of user soil and crop database was prepared and used as a bridge that connects the soil and land use map on one side and look-up table on the other side during land/soil/slope definition. After Land use, soil, and slope characterization were done each map of the watershed was overlaid to define a hydrologic response unit by setting a thresh hold for each map.

For this specific study a 5% threshold value for land use, 10% for soil, and 10% for slope were used. The HRU distribution in this study was determined by assigning multiple HRU to each sub-basin. For the recent year, 2020, 25 sub-basin and 75 HRUs were produced whereas for the year 2016 25-sub basin and 57 HRUs were created by integrating land use and land cover, soil, and slope maps. The full hydraulic response unit of the kulfo watershed for different year periods specified is shown in figure 3.9 below.

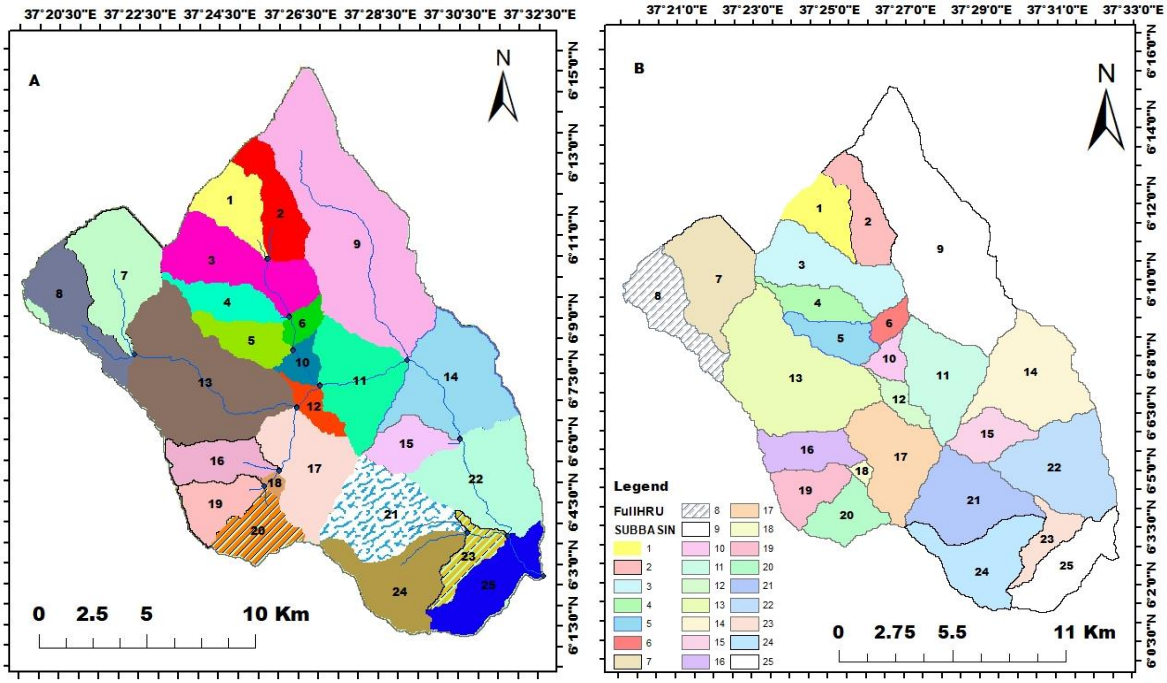

Figure 3.9 Full Hydrological Response Unit (HRU) Map of kulfo Watershed

Weather Data Definition

SWAT requires a long year's daily record of precipitation, maximum and minimum temperature, solar radiation, relative humidity, and wind speed.

The SWAT weather generator model (WXGEN) was used to fill missing values in weather data. Since most of the stations have no full weather data like that of relative humidity, solar radiation, and wind speed data by selecting one synoptic station which has full weather data SWAT generates the above data by using a weather generator. For this case, the Arba Minch station is a synoptic station that has full weather data and generates data for the other station. The Penman-Monteith method which utilizes the solar radiation, relative humidity, and wind speed data records were employed for the estimation of potential evapotranspiration (PET). Meteorological stations are also geo-referenced using latitude, longitude, and elevation data.

The weather generator collects all information of climate data in one folder then from this the data has been imported to the SWAT 2012 model database.

The last step before a SWAT simulation is going to be run is to write all of the input files required by SWAT and produced from the preprocessed data from Arc SWAT. Once they are written, individual files can be edited through Arc SWAT, or externally.

Model simulation

After the model is set up the next step is running the model and the model runs daily from the year 1991 to 2004 by letting 1-year warm-up period. The output result cannot be used for further analysis without evaluating the ability of the model to predict stream flow through sensitivity analysis, model calibration, and model validation.

3.7 Sensitivity Analysis

The first step in the calibration and validation process in SWAT is the determination of the most sensitive parameters for a given watershed or sub-watershed. Sensitivity analysis was performed on the SWAT model to identify the influential parameters on the modeled streamflow. It is important to identify sensitive parameters for a model to avoid the problem of over-parameterization.

Lenhart et al., (2002) described the importance of sensitivity analysis as to allow the reduction of a number of parameters that must be estimated, thereby reducing the computational time required for model calibration. Once the sensitivity analysis is done calibration can be performed for a limited number of influential parameters.

To improve simulation results and thus understand the behavior of the hydrologic system in the Kulfo watershed, sensitivity analyses were conducted using the entire flow parameters

for SWAT models. Therefore sensitivity analysis is used as an instrument for the assessment of the input parameters concerning their impact on model output (Lenhart et al. 2002).

The current version of the SWAT model, SWAT2012, provides algorithmic techniques for sensitivity analysis. Two types of sensitivity analysis are allowed when using SUFI2 (Sequential Uncertainty Fitting version 2). Global Sensitivity and One-at-a-time sensitivity analysis. The two aforementioned sensitivity analysis methods may yield different results since the sensitivity of one parameter depends on the value of other related parameters. In this study, global sensitivity analyses were performed and the ranking of the parameters was determined.

Table 3.5 Some of the Parameters and their description including maximum and minimum values

	Parameters	Description	Min	Max
1	SURLAG.bsn	Surface runoff lag time	0.05	24
2	SOL_ALB	Moist soil albedo	0	0.25
3	GW_DELAY	Ground water delay in days	0	500
4	REVAPMN	Threshold depth of water for revap to occur	0	500
5	SLSUBBSN	Average slope length	10	150
6	CH_N2	Average width of main channel	0	1000
7	RCHRG_DP	Deep aquifer percolation fraction	-1.35	0.18
8	CH_K2	Effective hydraulic conductivity in main channel alluvium	-0.01	500
9	SOL_AWC	Available water capacity of soil layer	0	1
10	EPCO	Plant uptake compensation factor	0	1
11	TLAPS	Temperature lapse rate	-10	10
12	CN_2	SCS runoff curve number	35	98
13	CH_ERODMO	Jan. channel erodibility factor	0	1
14	ALPHA_BF	Base flow alfa factor in days	0	1
15	GWQMN	Threshold depth of water for return flow to occur	0	5000

3.8 Model Calibration and Validation

Model calibration is an iterative exercise used to get the most suitable parameter in modeling. It involves the identification of the most important model parameters and changing the parameter set. The calibration was done on monthly time steps using the average measured streamflow of Kulfo catchment covering from January 1993 to December 2000. After the model was calibrated and got acceptable results the model was validated using measured data of average monthly streamflow of 4 years from January 2001 to December 2004.

Validation was done to compare the model outputs with an independent data set, that were set for the calibration process, without making further adjustments to the parameter values. The process continues till the simulation of the validation period of streamflow confirms best to the measured data of its correspondence so that the model performs satisfactorily. In the validation process, four-year flow data was used for all of the four land use land cover maps to evaluate the model accuracy.

Both model Calibration and validation were conducted by the SWAT Calibration and Uncertainty Program (SWAT-CUP) 2019, Version 5.2.1.1, which facilitates the calibration process (Arnold, et al., 2012). Among the available algorithm in the SWAT – the CUP SUFI-2 algorithm was used for model calibration, validation, and sensitivity analysis for this study. Among various evaluation coefficients allowed in SUFI-2, the Nash- Stutcliffe coefficient (NSE) was chosen for model optimization in SWAT-CUP.

3.9 Model Performance Evaluation

The performance of the model was evaluated by assessing the correlation between simulated and observed values using statistical measures. There are a lot of model statistical measures approaches available for instance Nash-Sutcliffe efficiency (NSE), Percent Bias (PBIAS), the ratio of the root mean square error to the standard deviation of measured data (RSR), and coefficient of determination (R^2).

The major statistical approaches for analyzing model performance used in this study were Nash-Sutcliffe efficiency (NSE) and coefficient of determination (R^2) because those approaches were widely used for model performance analysis.

The R^2 value is an indicator of the strength of the relationship between the observed and simulated values. R^2 ranges from 0.0 to 1.0 with higher values indicating better agreement (Legates and McCabe, 1999). And it is calculated using equation 3.1.

$$R^2 = \frac{\sum_{i=1}^{n}(Q_{obs} - \bar{Q}_{obs})(Q_{sim} - \bar{Q}_{sim})}{\sqrt{\sum_{i}^{n}(Q_{obs} - \bar{Q}_{obs})^2}\sqrt{\sum_{n}^{i}(Q_{sim} - \bar{Q}_{sim})^2}} \quad (3.1)$$

Where:- Q_{sim} and Q_{obs} are the simulated and observed values respectively, $\bar{Q}_{obs}$ Is the mean of n observed values and $\bar{Q}_{sim}$ is the mean of n simulated values

The other method was Nash-Sutcliffe efficiency (NSE) which is a normalized statistic that determines the relative magnitude of the residual variance compared to the measured data variance (Nash, 1970).

$$NSE = 1 - \frac{\sum_{i=1}^{n}(Q_{oi} - Q_{si})^2}{\sum_{i=1}^{n}(Q_{si} - \bar{Q}_{si})^2} \quad (3.2)$$

Where: - NSE = Nash- Stutcliffe coefficient, Q_{si} = Average measured discharge value (m3/s), Q_{obi} =Observed monthly discharge (m3/s), I = month observed and simulated.

According to Nash, (1970) the value of NSE varies from 1(perfect fit) to negative infinity, and values between 0.0 and 1.0 are generally viewed as acceptable levels of performance If NSE is negative, predictions are very poor which indicates unacceptable performance.

Another test was the RSR value (the ratio of the root mean square error (RMSE) to the standard deviation (STDEV) of measured data and calculated using Equation 3.3.

$$RSR = \frac{RMSE}{STDVE_{obs}} = \frac{\sqrt{\sum_{i=1}^{N}(Q_{obs,i} - Q_{sim,i})^2}}{\sqrt{\sum_{i=1}^{N}(Q_{obs,i} - \bar{Q}_{obs})^2}} \quad (3.3)$$

Where: - Qobs I is the observed streamflow (m3/s), $\bar{Q}_{obs}$ is the mean of the observed data, and N is the total number of observations.

The percent of bias (PBIAS) shows the gap of the simulation value from the measured value. Mainly it measures the average tendency of the simulated data to be larger or smaller than the observed one. The percent of bias (PBIAS) is calculated using equation 3.4

$$PBIAS(\%) = \frac{\sum_{i=1}^{N}(Q_{obs}^{i} - Q_{sim}^{i}) * 100}{\sum_{i=1}^{N}(Q_{obs}^{i})} \ldots\ldots\ldots\ldots\ldots\ldots\ldots\ldots\ldots\ldots\ldots eq(3.4)$$

The optimal recommended values for the measure of performance of the model are shown in table 3.6.

Table 3.6 General performance ratings for recommended statistics for a monthly time step (moriasi et al., 2007).

Performance Rating	RSR	NSE	PBIAS(%) for sediment
Very good	$0.00 \leq RSR \leq 0.50$	$0.75 < NSE \leq 1.00$	$PBIAS < \pm 15$
Good	$0.50 < RSR \leq 0.60$	$0.65 < NSE \leq 0.75$	$\pm 15 \leq PBIAS < \pm 30$
Satisfactory	$0.60 < RSR \leq 0.70$	$0.65 < NSE \leq 0.65$	$\pm 30 \leq PPBIAS < \pm 55$
Unsatisfactory	$RSR > 0.70$	$NSE \leq 0.50$	$PBIAS \geq \pm 55$

The overall flow and various approaches followed to achieve the research objectives are described as a flow chart in figure 3.10.

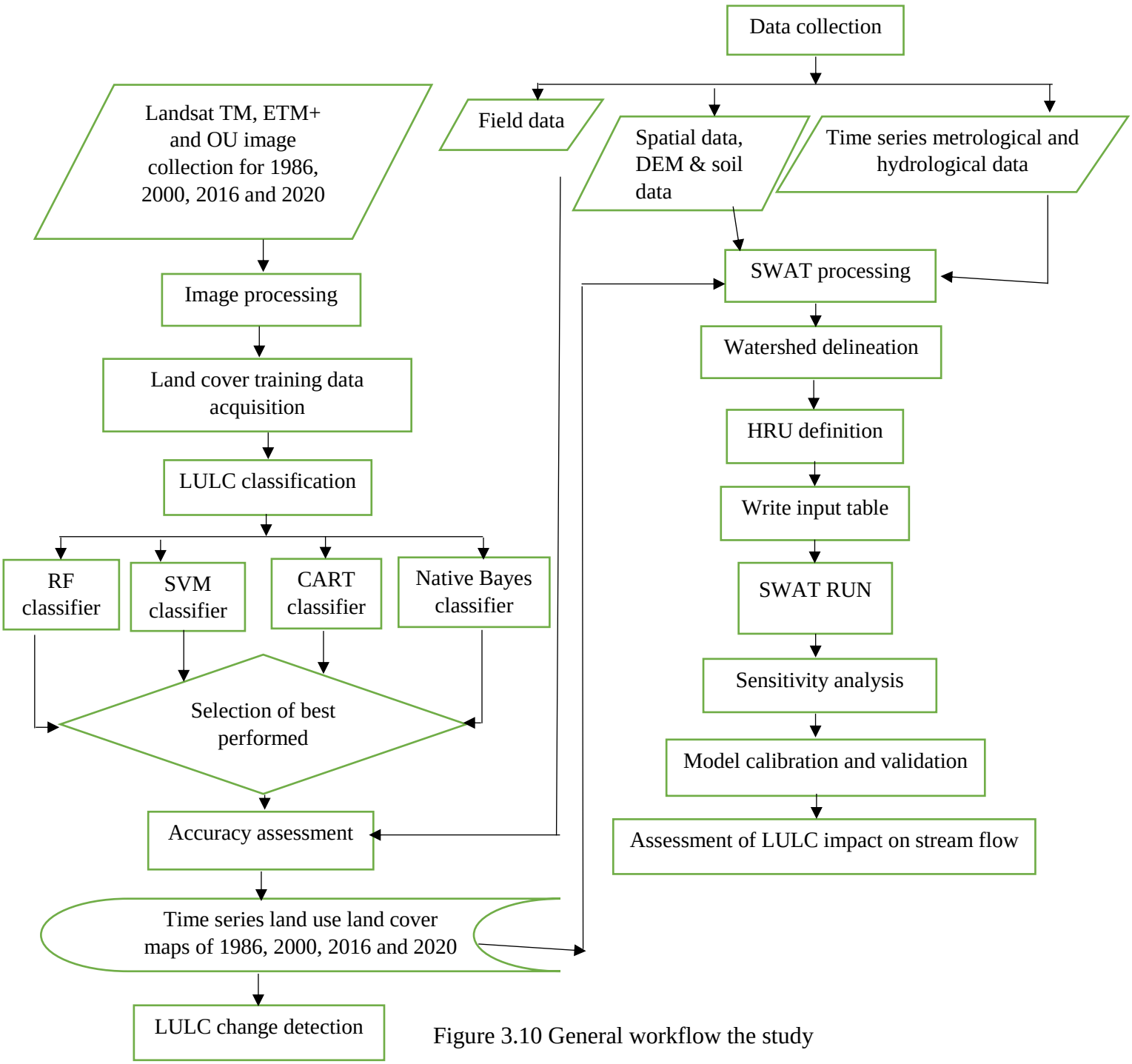

Figure 3.10 General workflow the study

4. RESULTS AND DISCUSSION

In this study, the google earth engine was used by implementing JavaScript for accessing, processing, performing the land use and land cover classification, and export the LULC maps which are detected from the Landsat Images. Accordingly, four machine learning classifiers (algorithms) that are widely used and available on GEE were applied and compared in LULC classification for the case of Kulfo catchment. However, based on their accuracies the best-outperformed algorithm was selected to generate time series LULC map of Kulfo catchment (1986, 2000, 2016, and 2020).

The accuracy of these maps was also evaluated corresponding to GCPs collected from the field (to compare the algorithms and for the time series LULC maps), Google Earth Image, and community information (for the time series LULC maps) using an error matrix and appropriate accuracy indices. The LULC change detection and the impact of the historical LULC change on streamflow were also presented in this section.

4.1 Comparison of Classifications using Different GEE Classifiers

In this study, four machine learning algorithms that were used for LULC classification were compared and evaluated. These classifiers, (RF, SVM, CART, and Naïve Bayes), are existed in the GEE. However, the accuracies and performance of these classifiers were evaluated corresponding to GCPs that were collected from the field using an error matrix.

The recent and free cloud cover Landsat image that was collected on the date of 2020-12-11 (https://earthengine.google.com) was used to classify and evaluate the algorithms in LULC classification for the case of Kulfo catchment.

4.1.1 Accuracy Assessment

The error matrix which is widely used to evaluate the accuracy of algorithms and methods used for LULC classification is applied in this study. However, the best-performed algorithm in the LULC classification was presented in Table 4.1. For the sake of clarity and reducing repetition, the error matrixes for the other Machin learning algorithms were described in **Appendix B.**

In the case of the SVM algorithm, the producer's accuracy was ranged from 53.33 % to 79.49 %. The algorithm was highly performed better in detecting the shrub land with 79.49% of accuracy, whereas the user's accuracy was ranged from 58.5% to 75% and it indicates the grassland detected as 75% off accuracy. High commission error was observed in the shrub land due to some of the shrub land pixels laid on the bare land features. The reason

for the occurrence of lower accuracy for these classes may be partly attributed to the horizontal spatial resolution (30m) of Landsat data (image) and generally smaller size of the feature areas as well as the sparse distribution of shrub land. This might confuse the algorithms in differentiating the shrub land and the bare lands. The overall accuracy of the algorithms was 86.71% and the statistical kappa coefficient was 0.861. This indicates that the algorithm ranged as very good (Taati et al., 2015).

Table 4.1 Error matrix of the LULC map of the Kulfo catchment which was classified using the SVM algorithm for 2020.

	Bare Land	Grass Land	Shrub Land	Mixed forest	Agricultural land	Vegetation	Users Accuracy	Commission error
Bare Land	34	0	5	0	11	0	68.0%	32.0%
Grass Land	0	30	0	1	9	0	75%	25%
Shrub Land	10	1	31	3	4	4	58.5%	41.5%
Mixed forest	3	2	1	30	2	5	69.8%	30.2%
Agricultural land	5	13	0	2	40	5	65.0%	35.0%
Vegetation	1	1	2	2	9	35	70	30%
Sum	53	47	39	38	75	49	67.7	
Producers Accuracy %	64.15	63.83	79.49	78.95	53.33	71.43		
Omission Error%	35.85	36.17	20.51	21.05	46.67	28.57		

In the RF algorithm, the user's accuracy ranged from 69.2% to 97.7%. The mixed forest has about 97.7% user's accuracy with 2.3% of commission error. And also, the producer's accuracy is ranged between 66.67% and 93.62%. Among the land features, vegetation land cover obtained 93.62% of producer's accuracy with 6.38% of omission error. In this Machin learning algorithm, a high commission error of about 30.8% has been noticed at agricultural land because more of the agricultural land pixels are classified as mixed forest as well as some are laid on other land feature classes. Among the land feature class, the algorithm faced a challenge in differentiating agricultural land features from the mixed forest. However, The overall accuracy was 79.73% and the kappa coefficient was 0.79. Even if this classifier performed less when compared to the SVM classifier the algorithm was still good in

detecting LULC for the case of the Kulfo catchment. The complete error matrix of this classifier is found in **Appendix D.**

In the case of the Naive Bayes algorithm, the percentage of user's accuracy was between 75 to 58.5 whereas producers' accuracy lays between 79.49% to 53.33%. Very high commission error occurs at shrub land around about 41.5%. This error occurs because some of the shrub land pixels were classified as bare land. This indicates that the Naive Bayes algorithm was not able to completely differentiate the shrub land and bare land feature class. In addition to this, some of the land feature classes share the pixel values of the shrub land. The overall and kappa coefficient of this algorithm were 66.4% and 0.64 respectively.

The final classifier was the CART algorithm this classifier got difficulty in classifying the shrub land and bare lands like that of the Naive Bayes algorithm. The producer's and user's accuracy range from 45.45% to 75.00% and from 56.6% to 70% respectively. The overall accuracy was 59.1% and the kappa coefficient was 0.58%. Based on the accuracy assessments CART algorithm was the least performed classifier out of the four machine learning classifiers.

In this study, the SVM machine learning algorithm was performed with better accuracy compared with other machine learning algorithms that were applied for LULC classification. Because kulfo catchment has a multi-feature and heterogeneous LULC cover class for this type of catchment SVM is the best type of classification algorithm.

Finally, the overall accuracy and kappa statistics of all Machine learning algorithms have been stated in table 4.5 below. Based on the summary result of accuracy assessment the best-outperformed classifier was support Vector Machines (SVM) which has produced a much higher accuracy of 86.71% for overall accuracy and 0.861 for kappa coefficient.

Table 4.2 Summary of Overall classification accuracies and kappa statistics achieved by GEE machine learning classifiers

Classifier	Overall Accuracy (%)	Kappa Statistics
Support Vector Machines(SVM)	86.71	0.861
Random Forest(RF)	79.73	0.79
Fast Naive Bayes	66.4	0.64
CART	59.1	0.58

For more clarity, the classified LULC map of kulfo catchment using four different classifiers was shown in **Appendix C**. In this study, the LULC map was classified into six different classes (bare land, grass land, shrub land, mixed forest, agricultural land, and vegetation cover) using GEE.

4.2 Historical LULC maps and Change detection

The machine learning algorithm which was performed better in detecting the LULC map for the case of Kulfo catchment was selected to generate a historical LULC map for 1986, 2000. 2016, and 2020.

4.2.1 Accuracy assessment

The LULC maps are not very useful without quantitative statements about their accuracy. The accuracy of the maps for the year 2020 is presented as an error matrix above in Table 4.1 and for other periods it is described in **Appendix D.** The numbers along the diagonal of the matrix indicate the number of reference pixels that are accurately classified by the algorithm. The values outside the diagonal were shows misclassifications. As shown in Table 4.1, the algorithm got difficulties during the classification of some of the land cover/use features. For example, agricultural land pixels were classified as grass Land, Bare land as well as a mixed forest because of the reflectance similarity of agricultural land with the described land use land cover types. In Addition to this among other land use land cover class more of the vegetation cover class fall under agricultural land class. This indicates that the algorithm has been confused in detecting (classifying) the agricultural land class and vegetation covers. For the map of 2020, the overall accuracy was 86.71% & the kappa coefficient was 0.861. The classification accuracies are in acceptable ranges compared to the recommended overall accuracy of at least 85% and the Kappa coefficient of 75%.

4.2.2 Land use and land cover change

In this section, change detection of Kulfo catchment for 34 years is performed based on the previous classification results of time series data. As a result (Figure 4.1) shown below shows the land use and land cover maps of the Kulfo watershed during 1986, 2000 2016, and 2020 that have been generated from Image Collection LANDSAT/LT05/C01/T1_SR, LANDSAT/LE07/C01/T1_SR, and LANDSAT/LC08/C01/T1_SR respectively.

After the image processing and land cover detection six (agricultural land, grassland, shrubland, mixed forest cover, bare land, and vegetation cover) land use and land cover classes were determined for the years 1986, 2000, 2016, and 2020 respectively.

As shown in figure 4.1A the spatial distribution of land use land cover class throughout the catchment has a great difference in the 1986 land use and land cover map. For instance, the upper part of the watershed was highly covered with grassland and agricultural land were as the lower part was dominated by bare land and shrub land. Besides this, an increasing trend of agricultural land from the upper to the middle of the catchment was recognized (noticed).

During the period 2000, the upper part was covered with agricultural land, and vegetation cover was slightly increased when compared with the period of 1986 (Figure 4.1A and B). In the upper part of the watershed not only the agricultural land the bare land was also slightly expanded with the reduction of grassland and shrub land. At the most downstream part of the watershed, the bare land was slightly reduced at the expansion of agricultural land. Moreover, the agricultural land expanded along the riparian of the catchment.

All in all, among the land use and land cover class the increment of agricultural land was highly noticed.

By the year 2016, a considerable increment of bare land mixed with shrub land was observed at the middle and lower part of the watershed (Figure 4.1C). And also plantation of Banana and avocado vegetables were recognized at the downstream part and along the riparian of the catchment which was not available on the previous maps.

The final period 2020 shows dramatically expansion of agricultural land all over the catchment (Figure 4.1D). In addition to this, the bare land and mixed shrub lands increased at the downstream right part of the catchment. The mixed forest above the middle part of the watershed increased this is because of the high plantation of false bananas.

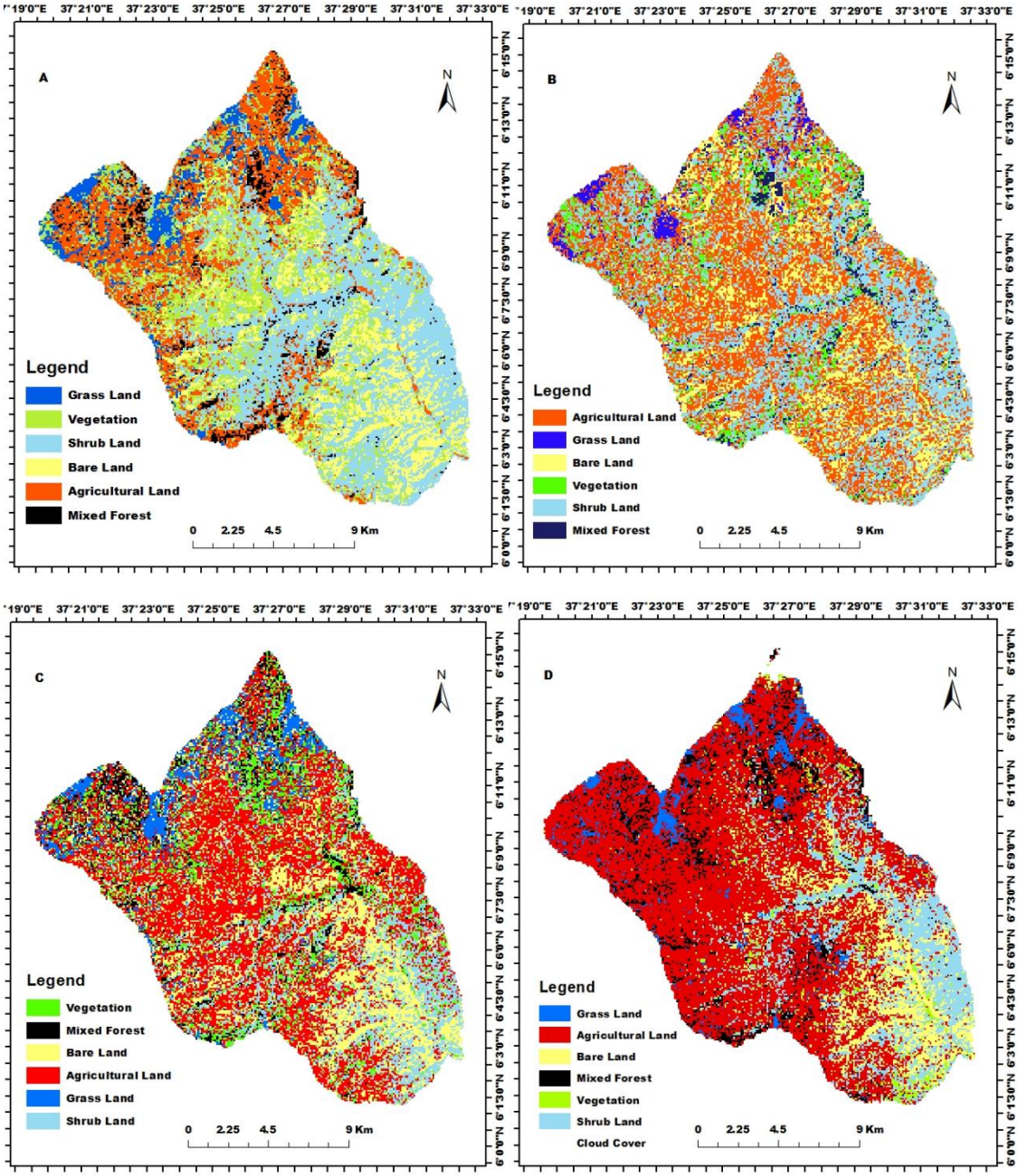

Figure 4.1 Classified land use/ cover map of Kulfo watershed for the year of A) 1986 B) 2000 C) 2016 D) 2020.

The land use and land cover map of 1986 (Figure 4.1A) and the percentage coverage of each land cover class (Table 4.6 and Figure 4.2) indicates that the Kulfo watershed is covered by 18.81% of vegetation land, 19.44% of agricultural land, 15.25% of bare land, 34.18% of shrub land, 0.4.34% of grassland and also 7.09% of mixed forest.

By the year 2000, the land cover map of 2000 (Figure 4.2B) and the percentage coverage of each land cover class (Table 4.6 and Figure 4.2) shows that the vegetation cover decreased to 7.26%, the agricultural land covers 39.48% of the watershed whereas 52.33% of the

watershed was occupied by other land use land cover types. During this period, vegetation, grassland, mixed forest, and shrub land in the catchment were mainly reduced. In contrast, the agricultural land was expanded in most parts of the catchment.

Similarly, about 47.95% of the watershed was dominantly coved by agricultural land, 20.55% by bare land, 15.92% by shrub land, and around 15.6% occupied by other types of land use land cover types during 2016 (Table 4.6 and Figure 4.2).

The recent year 2020 LULC map (Figure 4.1D) and the percentage coverage of each land cover class (Table 4.6 and Figure 4.2) shows that the catchment was covered by 57.12% of agricultural land, 11.68% of bare land, 14.73% of shrub land, 4.06% of grassland and 8.66% of mixed forest. In this recent land use map, some parts of vegetation, mixed forest, grassland, and shrub land were reduced and replaced mainly by agricultural land.

The spatial analysis result of the land-use dynamics was summarized as follows in Figure 4.2 and tabular form in Table 4.6. So, that it is simple to compare land use/land cover change patterns and the overall land-use dynamics with time.

Table 4.3 Area coverage of each land use/cover type.

	1986		2000		2016		2020	
LULC types	Km^2	%	Km^2	%	Km^2	%	Km^2	%
Vegetation	59.63	18.81	23.01	7.26	20.23	6.38	9.84	3.10
Agricultural land	61.614	19.44	125.14	39.48	151.978	47.95	181.025	57.12
Bare Land	48.433	15.28	50.83	16.04	65.123	20.55	37.006	11.68
Shrub Land	108.34	34.18	97.99	30.92	50.452	15.92	46.69	14.73
Grass Land	13.89	4.38	9.4508	2.98	15.26	4.81	12.88	4.06
Mixed Forest	25.025	7.90	10.503	3.31	13.97	4.41	27.45	8.66
Cloud Cover	0	0.00	0	0.00	0	0.00	2.03	0.64

Figure 4.2 shows the area coverage of each LULC in Kulfo watershed for different years' time periods including land use/cover of 1986, 2000, 2016, and 2020 year.

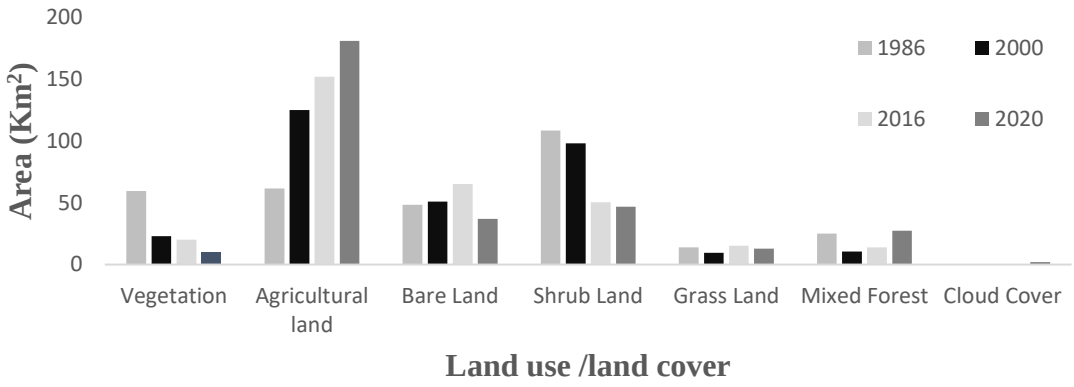

Figure 4.2 the area coverage of land use/cover change in Kulfo catchment.

4.2.3 Land use and land cover change detection

A change detection map that provides "from–to- class" change information was produced for each class of the study area. Figure 4.3 shows the changed land use and a land cover class of the study area indicated with a variety of different colors.

As shown in figure 4.3A during the year (1986 -2000) among the classified types of land use land cover class the bare land and vegetation covers have been more decreased and converted to agricultural land. Specifically, the upper part of vegetation and at the same time, bare land situated at the middle part of the watershed were changed to agricultural land.

Figure 4.3 B describes the land use and land cover class of the year 1986-2016, during this period the grassland and bare land converted almost to agricultural land. Moreover, the shrub land has been lost due to the changing of it to agricultural land. From this trend, one can conclude that agricultural activity was very high during this period.

At the same time figure, 4.3 C and D major losses were noticed in shrub land, vegetation cover and bare land whereas gain was observed in agricultural land.

All in all, the analysis of LULC for the study watershed revealed that agricultural land was predominant and showed slight continuous increment over the studied period (1986 -2020). In addition to figure 4.3, table 4.4 shows clearly the areal coverage of each land use land cover class.

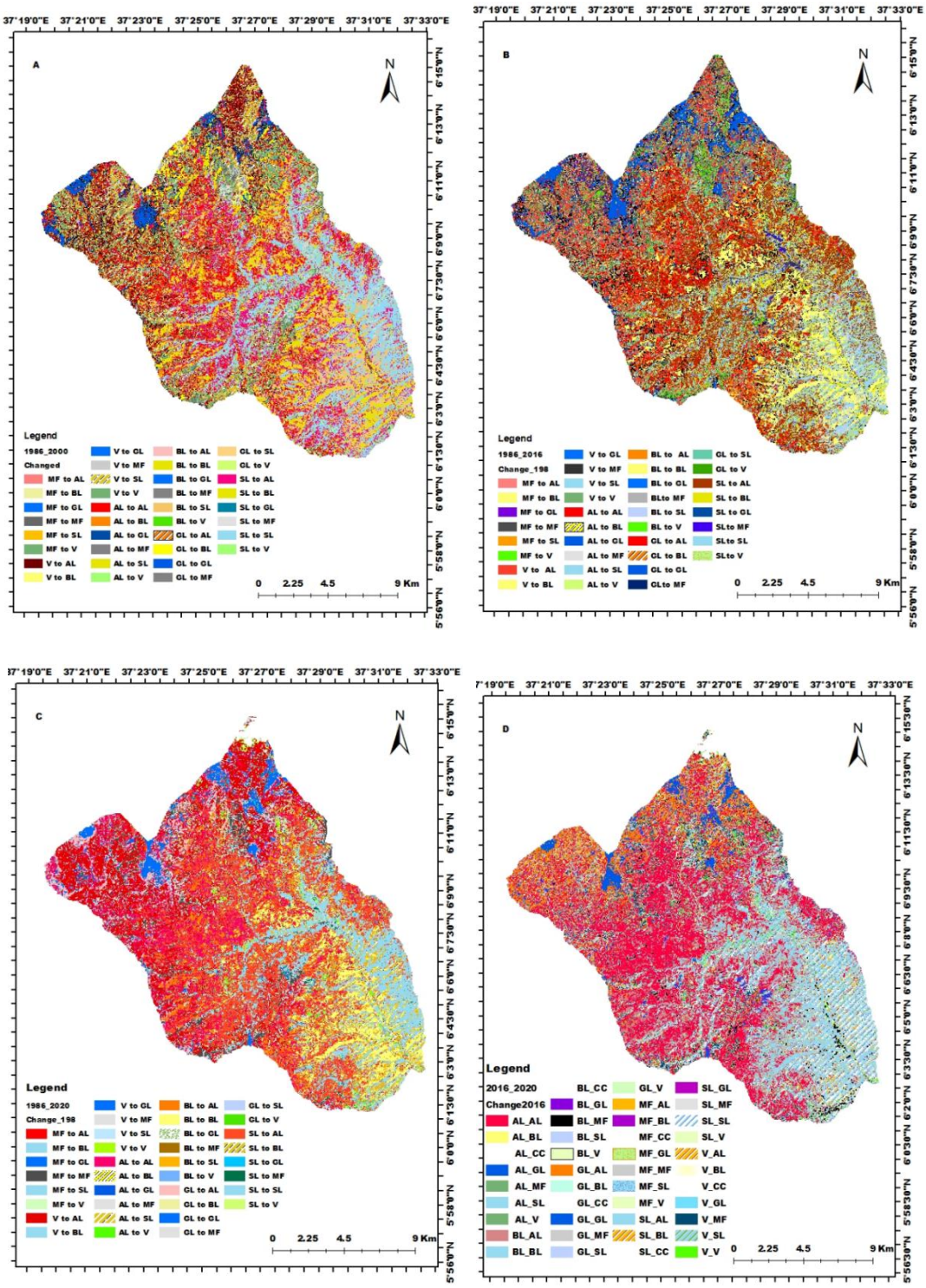

Figure 4.3 Land use land cover change dynamics for the period A) 1986 to 2000 B) 1986 to 2016 C) 1986 to 2020 D) 2016 to 2020.

Table 4.4 Major changes in LULC classes from the period of 1986 to 2020 in the area and percentage coverage in the Kulfo watershed.

LULC	Changed To	1986 - 2000		1986 - 2016		1986 - 2020		2016 - 2020	
		Area (km^2)	%	Area (km^2)	%	Area (km^2)	%	Area (km^2)	%
AL	AL	36.855	11.628	34.2405	10.803	45.264	14.373	97.218	30.870
	GL	1.7055	0.538	3.5271	1.113	2.4489	0.778	1.497	0.475
	BL	9.8334	3.103	11.6568	3.678	3.9042	1.239	4.555	1.446
	MF	0.1737	0.055	1.818	0.574	2.1132	0.671	3.174	1.008
	V	1.0251	0.323	2.5101	0.792	2.097	0.666	4.282	1.360
	SL	9.4788	2.991	5.319	1.678	2.97	0.943	13.031	4.138
GL	AL	6.7608	2.133	3.0744	0.970	11.634	3.695	11.660	3.702
	GL	5.8599	1.849	11.2806	3.559	6.511	2.067	7.340	2.331
	BL	5.4108	1.707	3.0753	0.970	0.161	0.051	0.347	0.110
	MF	0.1539	0.049	0.7146	0.225	0.847	0.269	0.227	0.072
	V	0.441	0.139	0.9216	0.291	0.197	0.063	0.362	0.115
	SL	0.8793	0.277	0.4392	0.139	0.089	0.028	0.151	0.048
BL	AL	17.9577	5.666	11.7864	3.719	21.02	6.674	32.699	10.383
	GL	0.0882	0.028	1.1178	0.353	1.007	0.319	2.618	0.831
	BL	25.137	7.931	26.9442	8.501	20.068	6.372	24.548	7.795
	MF	0.0225	0.007	0.0117	0.0036	0.055	0.017	0.614	0.195
	V	0.1107	0.034	0.3447	0.109	1.037	0.329	0.805	0.255
	SL	4.1445	1.308	7.2558	2.289	4.271	1.356	3.161	1.004
MF	AL	1.1079	0.350	1.6317	0.515	4.657	1.479	5.377	1.707
	GL	0.0108	0.003	0.0468	0.015	0.038	0.012	0.581	0.185
	BL	0.2691	0.085	0.2898	0.091	0.071	0.023	0.071	0.023
	MF	3.8034	1.200	5.2092	1.644	6.506	2.066	10.130	3.217
	V	5.166	1.630	4.7538	1.499	0.244	0.077	0.422	0.134
	SL	4.8132	1.519	3.2391	1.022	3.372	1.071	2.842	0.902
V	AL	23.9913	7.570	27.6111	8.712	44.466	14.119	14.539	4.616
	GL	1.3392	0.422	3.2211	1.016	1.301	0.413	0.423	0.134
	BL	2.1537	0.679	5.3136	1.676	0.947	0.301	0.345	0.109
	MF	2.4363	0.768	8.3727	2.642	14.567	4.625	9.797	3.111
	V	13.5702	4.282	16.8561	5.318	3.173	1.007	2.007	0.637
	SL	25.236	7.962	7.3521	2.320	2.980	0.946	8.627	2.739
SL	AL	38.4489	12.131	46.08	14.539	54.025	17.154	19.575	6.216
	GL	0.4878	0.154	0.9639	0.304	1.595	0.506	0.441	0.140
	BL	8.0739	2.547	17.3268	5.467	11.825	3.755	7.112	2.258
	MF	3.942	1.244	3.852	1.215	3.363	1.068	3.507	1.114
	V	2.637	0.832	10.7775	3.401	3.107	0.987	1.976	0.628
	SL	53.4132	16.853	28.0026	8.835	32.999	10.478	18.868	5.991

LULC=land use and land cover; AL=Agricultural Land; GL=grass land; MF= Mixed forest; BL=bare land; V = Vegetation; SL = Shrub Land; Km^2 = square kilometer (unit).

In the first period (1986-2000) about 2.133% grassland, 5.666% bare land, 0.349% mixed forest, and 12.13% vegetation cover were converted to agricultural land (Table 4.4). Conversely, about 7.01% (22.2165Km^2) of agricultural land was converted to other LULC types in the same period (1986-2000).

Due to the rapid increase of agricultural activity in the area about 46.08km^2 (14.539%) shrub land, 27.611km2 (8.722%) vegetation covers, and 11.7864Km^2 (3.719%) bare land was converted to agricultural land whereas 17.3268km^2 (5.467%) shrub land was converted to bare land during the year 1986 to 2016 (Table 4.4).

Similarly, the areas experienced the most severe loss of shrub and vegetation covers between the periods of 1986 – 2020. About 54.0252km2 of shrub land, 44.4654km2 vegetation, 21.0195km2 of bare land, and 11.6361 km^2 of grassland were altered to Agricultural land conversely 13km^2 agricultural land converted to other types of land use land cover class (Table 4.4).

4.3 Streamflow evaluation

SWAT CUP 2012 was used for sensitivity analysis and Sensitivity analysis was done by considering 30 flow-related parameters to identify which model parameter is top sensitive that has a significant influence on controlling streamflow in Kulfo watershed. Some of the parameters are CANMX, HRU_SLP, GW_REVAP, SURLAG, SOL_AWC, CN2, and more others.

4.3.1 Flow Simulation and sensitivity analysis

Sensitivity analysis of simulated streamflow for the watershed was performed using monthly observed streamflow using the SUFI2 program. Flow sensitivity analysis was carried out for a period of Thirteen years, which includes both two years of warm-up periods (from January 1, 1991, to December 31, 2004) and the calibration period (from January 1, 1993, to December 31, 2000). About 300, iteration has been done using SUFI2 program for flow calibration, and 27 parameters were reported as sensitive in different degree of sensitivity for streamflow. Out of 27 flow parameters, only selected top sensitive ones (Table 4.12 and **Appendix E**) were identified for the model to avoid model over parameterization. Table 4.12 shows the most sensitive parameters for the 1986 year of LULC map. For the map of 2000, 2016, and 2020 the most sensitive parameters are presented in **Appendix E.**

Table 4.5 Sensitive parameters and their rank in Kulfo catchment using 1986 LULC map.

No.	Parameter Name	t-Stat	P-Value	Rank
1	V__GWQMN.gw	-8.783	$1.94 * 10^{-16}$	1
2	V__GW_DELAY.gw	-3.94	0.000103	3
3	R__SOL_ALB (...).sol	-3.58	0.0004	4
4	R__HRU_SLP.hru	-2.4	0.02	5
5	A__SOL_AWC (...).sol	1.61	0.11	8
6	R__CN2.mgt	0.33	0.74	8
7	V__ALPHA_BF.gw	-0.13	0.90	10
8	R__GW_REVAP.gw	0.08	0.94	11

4.3.2 Calibration and validation

Based on the sensitive parameters calibration and validation of a flow was conducted for 1986, 2000, 2016, and 2020 LULC maps using observed streamflow by dividing the recorded streamflow data into two parts for calibration and validation.

LULC of 1986, 2000, 2016, and 2020 was calibrated for 7 years from January 1993 to December 2000 and Validated for an independent period of 4 years from January 2001 to December 2004.

The result of model performance during calibration and validation period of monthly streamflow demonstrated a good agreement between observed and simulated streamflow with the following coefficient of determination (R^2) and Nash-Sutcliffe efficiency (NSE) for land use and land cover map of 1986, 2000, 2016 and 2020 (Table 4.6).

Table 4.6 Model performance measures for calibration and validation.

Land use and land cover map	Calibration		Validation	
	R^2	NSE	R^2	NSE
1986	0.75	0.6	0.8	0.72
2000	0.76	0.8	0.75	0.6
2016	0.79	0.75	0.73	0.74
2020	0.81	0.75	0.8	0.75

Table 4.8 indicates the results of the simulation of the flow for the model performance that is adequately good during the calibration and validation periods. This indicates that the model performs well in simulating the generated streamflow from the catchment.

Therefore, the simulation results can be used in assessing the LULC impacts on streamflows.

In addition to the above statistical measures, the following line graph shows the relationship between observed and simulated streamflow during calibration and validation of LULC maps of the years 1986, 2000, 2016, and 2020. As we can see from the graph there was a great relation between stream flows observed and simulated.

The hydrography of 1986 LULC is not normally distributed because the mean and median values are not equal there value is 6.723m3/s and 6.11 respectively. The majority of the simulated streamflow was observed from Jan 1994 up to December 2000. There is a long tail on the right-hand side of the mean value as the tail is on the positive side of the hydrograph mean value the streamflow distribution is positively skewed with the value of 2.0. The same is true for all LULC maps of 2000 and 2020 except for 2016 of streamflow hydrographs the mean value of the simulated streamflows were 7.94m^3/s and 7.86m^3/s whereas the values of skewness were 2.37m^3/s and 2.59m^3/s respectively. However, the streamflow hydrograph of generated from the LULC map of 2016 is different because its mean value is very large which has 10.11m3/s, and also the shape of the hydrograph is more skewed to the right by 1.02. Generally, it can be observed that as the agricultural land increases the hydrograph looks flatter.

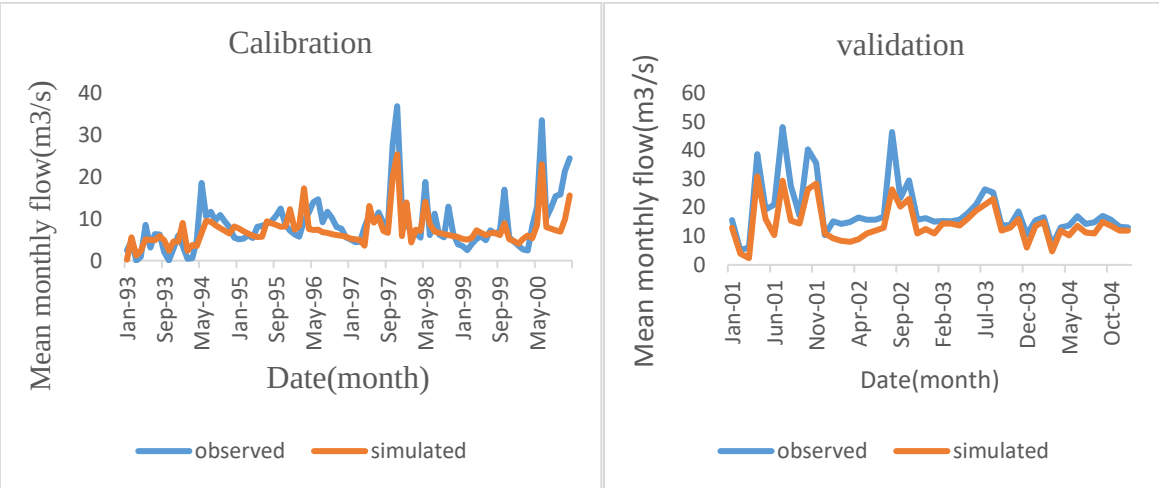

Figure 4.411 Model Calibration and validation period for LULC 1986

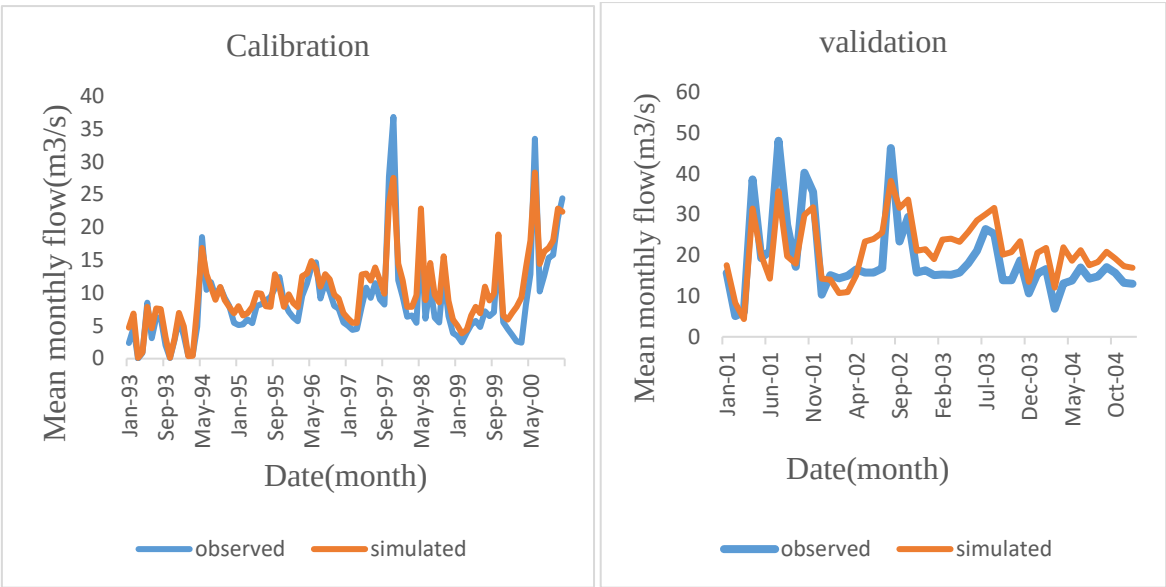

Figure 4.5 Model Calibration and validation period for LULC 2016.

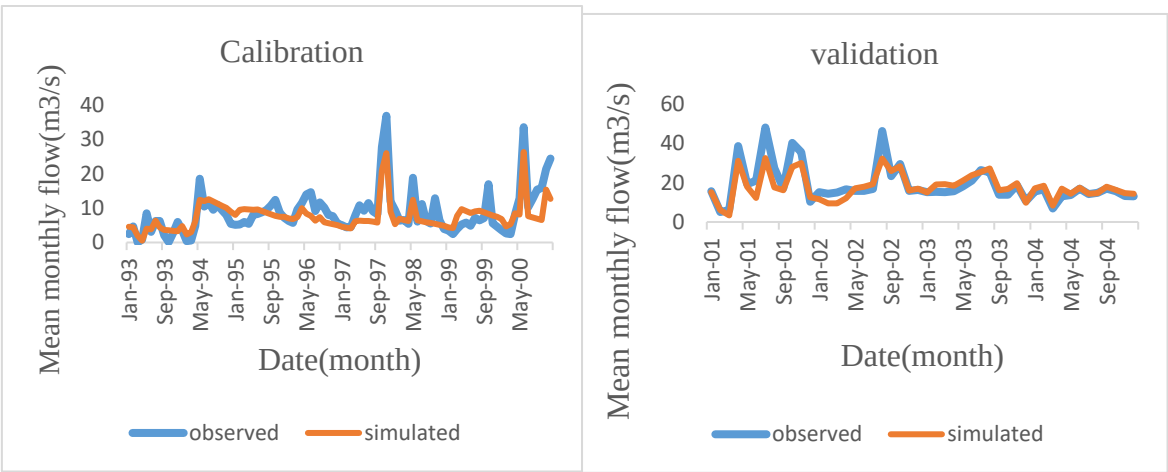

Figure 4.6 Model Calibration and validation period for LULC 2000.

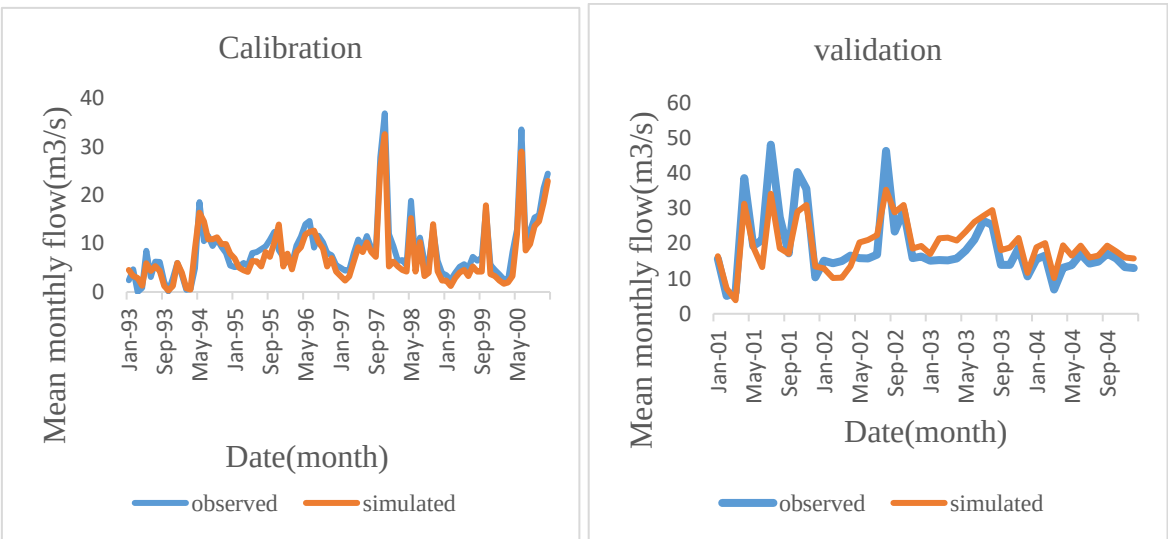

Figure 4.7 Model Calibration and validation period for LULC 2020.

4.4. Impact of land use and land cover change on streamflow

The main aim of this study was to assess the impact of land use and land cover changes on stream flows of Kulfo catchment. For this purpose, four different land use land cover maps were generated and used to produce four different SWAT model simulations.

4.4.1 Change on Monthly streamflow

Table 4.7 Monthly streamflow change for the study period

	Jan	Feb	Mar	Apr	May	Jun	Jul	Aug	Sep	Oct	Nov	Dec	Average
1986	3.60	2.72	3.36	5.06	8.37	11.49	8.85	7.90	7.17	8.2	8.89	5.05	6.72
2000	5.67	5.40	5.73	7.10	9.00	10.28	7.94	7.59	7.70	9.89	6.57	5.70	7.38
2016	7.01	5.84	5.88	9.09	9.66	11.99	12.66	11.64	10.55	7.98	8.96	9.92	9.265
2020	4.70	3.03	3.59	5.17	10.00	10.30	10.70	9.89	10.97	8.96	9.69	7.14	7.85

By the year 1986 the average monthly flow was low relative to other years this is due to the effect of shrub land which had very higher coverage on the catchment about 34.18% of the catchment (Table 4.4). The shrub land has high porosity and will delay the flow of water to the outlet of the catchment. Hoverer, the shrub land has been reduced by 30.92% at the year of 2000 with a complete increment of agricultural and bare land at the same time the streamflow increased from 6.72m3/s to 7.38m3/s (Table 4.4). This indicates that the increase of agricultural activity and conversion of land use and land cover class to bare land was responsible for the occurrence of this change on streamflow from the period of 1986 to 2000. Similarly, between the years 2000 to 2016, there was an increase of streamflow by 25.53%. During this period, both bare land and agricultural land have been increased (Table 4.4).

At the same time during the periods of 2016 to 2020 the reduction of streamflow was noticed from 9.265 to 7.85m3/s by 15.33%. At this period, the dominant land use land cover class was agricultural land. Agricultural land use more water and doesn’t let the rainfall reach the outlet of the catchment because they have more porous media.

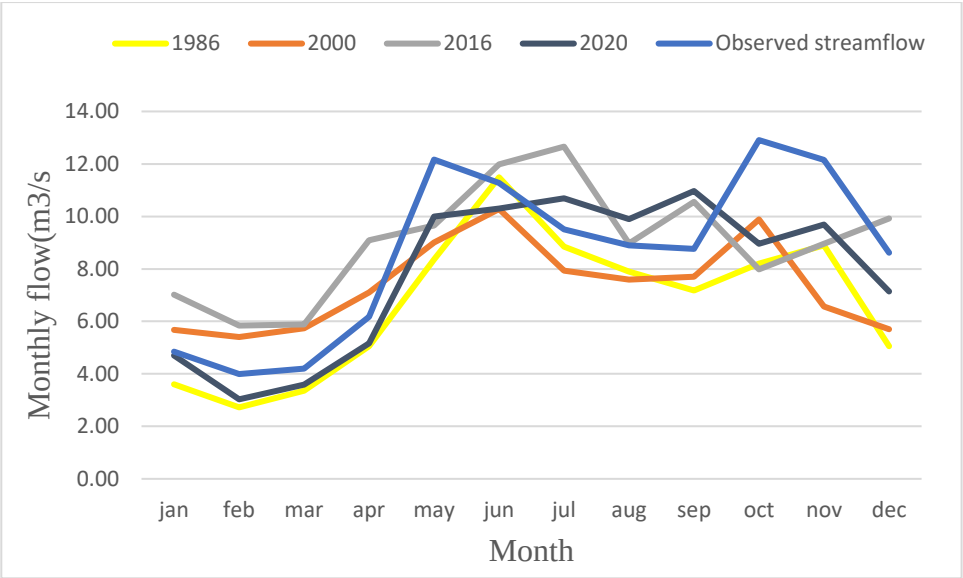

Figure 4.8 Monthly streamflow change over the study years.

4.4.2 Change on Seasonal Streamflow

For the analysis of seasonal streamflow, the months of Feb, Mar, Apr, and May are considered as Belg season whereas Jun, Jul, Aug, and Sep are taken as Kiremt season additionally months Oct, Nov, Dec, and Jan are assigned for Bega season.

The seasonal streamflow showed in Tables 4.8 and 4.9 shows great variation throw-out the three seasons because of LULC change. During Kiremt season, moderate decreases occurred between the years 1986 to 2000 by 5.366%. During this year, except for agricultural land and bare land, all land features have been decreased. The increment of agricultural land was very high this, in turn, will consume more water leading to decreasing in streamflow in the catchment. The effect of LULC change was largest in Kiremit season from 2000 through 2016. During this period, two LULC features, vegetation, and bare land have been decreased and increased respectively. This change made streamflow increase by 39.78% in return. At the same time the smallest seasonal change was noticed in Bega season the stream flow increased from 1986 to 2000 by 8.12% and from 2000 to 2016 it increased by 7.62%. However, the streamflow has more reduced by 9.985 between the years 2016 to 2020 due to a considerable reduction in all land features except the agricultural land and mixed forest. However, for the year 1986-2000, the effect on streamflow varies in Belge season increased by 39.57% whereas decreased by 28.49%.

Generally, the streamflow has decreased trend from 2016 to 2020 for all of the seasons whereas there was an increasing trend for the period of 2000 to 2016.

Table 4.7 Seasonal mean monthly flow (m3 /s).

	Kiremt season	**Belge season**	**Bega season**
1986	8.8525	4.8775	6.435
2000	8.3775	6.8075	6.9575
2016	11.71	7.6175	8.4675
2020	10.465	5.4475	7.6225

Table 4.9 Percentage of mean monthly flow change (m3 /s).

	1986-2000 (%)	2000-2016 (%)	2016-2020 (%)
Kiremt season	-5.366	39.779	-10.6319
Belge season	39.569	11.898	-28.487
Bega season	8.12	21.7	-9.98

5. CONCLUSION AND RECOMMENDATIONS

5.1 Conclusion

In this study, the output of the google earth engine and hydrological model has been used to evaluate the impacts of land use land cover change on streamflow of the kulfo watershed.

Land use and land cover change were detected in the past 34 years from 1986 to 2020 in Kulfo catchment. Agricultural lands constitute the largest portion of the watersheds and increase from year to year because of increasing consumption of land use and cover due to population growth.

For the land use and land cover analysis, all data/images were acquired, processed, and analyzed in the GEE platform using a raw satellite image of Landsat 5 TM, Landsat 7 ETM+, and Landsat 8 OLI with 30m of spatial resolution for preparing land use land cover map of 1986, 2000, 2016 and 2020. Since, GEE does not provide post-classification and comparison the change detection was performed on separate software, ArcGIS.

Before classification of Landsat image pre-processing and processing was conducted for better classification and accuracy result. Among the applied machine learning classifier algorithms SVM performed better and it has the highest overall accuracy of 86.71% and kappa coefficient of 0.861.

The accuracy of the prepared land use and land cover was done using confusion matrixes which measure the degree of agreement correspondence to the reference data. The values of all the accuracy indicators were within the acceptable range of values. Therefore, the accuracy of the four maps was found adequate to use the maps for further analysis as per the objectives of this thesis.

The land use land cover analysis clearly shows that bare land, vegetation, and shrub land were accompanied by the increase of agricultural land. This shows that agricultural activity within the catchment is very high this, in turn, will affect the natural resources in particular the hydrological cycle in general.

The results in this study indicate that there is a noticeable change in the LULC of the Kulfo catchment over the past decades.

Streamflow from the catchment was determined from the SWAT model. The model simulated for different land use land cover maps each of the maps give a different result and the performance of the model has been perfectly measured using model evaluation statistics

for each of the simulated streamflow, as result for the land use land cover map of 1986 NSE and R^2 values for the calibration period was NSE = 0.6 and R^2 = 0.75 whereas for the validation period NSE was 0.72 and R^2 0.8. For the year of 2000 land use land cover map, it is completely different the NSE becomes 0.8 and R^2 was 0.76 for the calibration period but for the validation period NSE was 0.6 and R^2 was 0.75. The value of NSE was 0.75 and R^2 0.79 for the calibration and NSE was 0.74 and $R^2$0.73 for validation for the year 2016.

For the recent year 2020, the NSE was 0.75 and R^2 0.81 and NSE was 0.75 and R^2 0.8 for calibration and validation periods respectively.

All of the model performance measures described above were in the acceptable range therefore SWAT model has perfectly simulated the streamflow in kulfo catchment.

The average monthly stream flows of the Kulfo catchment reduced from the year 1986 to 2000 by 30.92%. At the same time, the average streamflow increased by 25.53% during the year 2000 to 2016. During the recent period, the reduction of average streamflow was noticed by 15.33% from 9.265 to 7.85m3/s. The reduction of streamflow between the years 2016 and 2020 was may be due to a high percentage increase of bare land, a high percentage decrease of shrubs and grassland.

To analysis, the impact of LULC cover change on seasonal streamflow the months of the years have been divided into three seasons that are Kiremt, Belge, and Bega. There was a remarkable change in seasonal streamflow. The streamflow has decreased trend from 2016 to 2020 for all of the seasons whereas there was an increasing trend for the period of 2000 to 2016. Thus, the land use land cover change has affected the streamflow on kulfo catchment.

5.2 Recommendations

Based on the method and obtained results in this study some recommendations were stated as follow:-

1. The satellite data used has a spatial resolution of 30m with this resolution it is difficult to detect changes within the study area because the pixel values of each land use and land cover feature may be misclassified. These misclassified pixels are also caused by the limitation of a seasonal dataset of the area. However, for future studies, it is recommended to perform more accurate analysis at the micro-level with fine resolution data with ground truth details. An object-based classification and a fusion on spectral

indices need to be included and should also be considered to improve the accuracy of classification.

2. For validation of simulation result from the model one third of the historical stream data obtained from MOWIE has been used but it is better if measured stream flow data from the site is used for more representation and analysis of the changes.
3. The research was conducted by evaluating the effects of LULC changes on streamflow. However, the effects of LULC also have an impact on the component of streamflow of the catchment by changing the magnitude of surface runoff and groundwater flow. So, further research of this kind can be computed on the assessment of the impacts of LULC on streamflow components (surface run-off, base flow, and groundwater) analysis for the monthly and seasonal.
4. The soil data has been obtained from the Ministry of Water Irrigation and Electricity, Ethiopia, the spatial resolution of the soil map was very high this, in turn, leads to the reduction of the model performance in simulation. So, further research of this kind can get primary (filed data) so that the accuracy and the performance of the model will increase.
5. To evaluate the effect of LULC change on seasonal streamflow, it is important to first consider and identify the rainfall pattern because a rainfall pattern varies from place to place, and from time to time, this type of situation has not been studied in this study. Instead, information about the seasonality of rainfall patterns on kulfo catchment has been taken from previous studies and articles, so if the rainfall conditions are carefully studied, the current output and many other things can be improved. The analysis of the rainfall pattern to get a better result on the variability of seasonal streamflow was strongly recommended.

REFERENCES

A. Midekisa, F. H. (2017, september 27). Mapping land cover change over continental Africa using Landsat and Google Earth Engine cloud computing. doi: https://doi.org/10.1371/journal.pone.0184926.

A. Shelestov, M. L. (2017, Feb, 24,). Exploring Google Earth Engine Platform for Big Data Processing: Classification of Multi-Temporal Satellite Imagery for Crop Mapping,. *Front. Earth Sci,*. doi: https://doi.org/10.3389/feart.2017.00017.

Acharya, S., Pawar, S., & Wable, N. (2018, Apr). Application of Remote Sensing & GIS in Agriculture. *International Journal of Advanced Engineering Research and Science (IJAERS), Vol-5*(Issue-4).

Addis, H. K. (2016). Modeling streamflow and sediment using SWAT in the Ethiopian Highlands. . *I.nt J Agric & Biol Eng, Vol.9*, pp.51－66.

Ahmed, G. (2001). *Mapping a Dry Shrub Forest for Biodiversity Conservation Planning. (A case study in the salt range of Pakistan, using remote sensing and GIS tools).* Enschede, Netherlands: Forest Science Division, the International Institute for Geoinformation Science and Earth Observation (ITC).

ALI, H. (2009). *Land use and land cover change, drivers and its impact: A comparative study from Kuhar Michael and Lenche Dima of Blue Nile and Awash Basins of Ethiopia.* CornellUniversity.

Aneseyee, A. B., Elias, E., Soromessa, T., & Feyisa, G. L. (2019, December 9). Land use/land cover change effect on soil erosion and sediment delivery in the Winike watershed, Omo Gibe Basin, Ethiopia. (O. Wei, Ed.) *Science of the Total Environment*.

Arnold J. G., S. R. (1989). Large area hydrologic modeling and assessment, Part I: model development. *Journal of American Water Resources Association,, Vol. 34*, pp. 73-89.

Arnold, J. G. (2012). Soil and water assessment tool theoretical documentation version 2012. *Texas Water Resources Institute.* .

Arnold, Moriasi, D. N., Gassman, P. W., Abbaspour, K. C., White, M. J., Srinivasan, R., & C. Santhi, R. D. (2012). SWAT: MODEL USE, CALIBRATION, AND VALIDATION. *American Society of Agricultural and Biological Engineers ,,* P.1493.

Asitatikie, A. N. (2019). Impact of Land Use/Land Cover Change on Hydrology of the Catchment: The Case of Upper Ribb Catchment, Lake Tana Sub Basin, Ethiopia. *Journal of Environment and Earth Science, Vol.9*.

Assen, M. (2011). Land Use/ Cover Dynamics and Its Implications In The Dried Lake Alemaya Watershed, Astern Ethiopia. *Journal of Sustainable Development in Africa, V.13*(No.4).

Assessment of The Effects Of Climate Change On Land Use And Land Cover Using Remote Sensing: A Case Study From Kenya, DNC2015/03.

Assfaw, A. T. (2019, November 18). Calibration, validation and performance evaluation of swat model for sediment yield modelling in megech reservoir catchment, ethiopia. *Journal of Environmental Geography*.

Ayana, A. B., Chemeda, E. D., & Ekasit, K. (2012). Simulation of Sediment Yield using SWAT Model in Fincha Watershed, Ethiopia. 283 - 297.

Ayele, G. T. (2016). Multitemporal Land Use/Land Cover Change Detection for the Batena Watershed, Rift Valley Lakes Basin, Ethiopia.

Ayodele, T. O. (2010). Types of Machine Learning Algorithms, New Advances in Machine Learning,. *Yagang Zhang (Ed.),*.

Bahari, N. I., Ahmad, A., & Aboobaider, B. M. (2014). Application of support vector machine for classification of multispectral data. *7th IGRSM International Remote Sensing & GIS Conference and Exhibition.* IOP Conf. Series: Earth and Environmental Science.

Berhan, G. H. (2011). Using Satellite Images for Drought Monitoring: A Knowledge: A Knowledge Discovery Approach. *Journal of Strategic Innovation and Sustainability,, 7 (1),*, 135-153.

Berihun, M., Tsunekawa, A., Haregeweyn, N., Meshesha, D., Adgo, E., Tsubo, M., . . . Sultan, D. (2019). Exploring land use/land cover changes, drivers and their

implications in contrasting agro-ecological environments of Ethiopia. *Land Use Policy*, 87.

Betrie, G. D. (2011). Sediment management modelling in the Blue Nile Basin using SWAT model. *Hydrology and Earth System Sciences,*, 15(3), 807-818.

Bharti, L. T. (2020). Modelling sediment yield of Rib watershed,Northwest Ethiopia,. *ISH Journal of Hydraulic Engineering,*.

Bittencourt, H. R., & Clarke, R. T. (2003). Use of Classification and Regression Trees (CART) to Classify Remotely-Sensed Digital Images. *IEEE*.

Blainski, É., Porras, E. A., Garbossa, L. H., & Pinheiro, A. (x2016, November 27). Simulation of land use scenarios in the Camboriú River Basin using the SWAT model. *Brazilian Journal of Water Resources*.

Breiman, L. (2001). Random Forests. *Mach. Learn*(45), PP. 5–32.

Breiman, L. (pp. 5-32). Random Forests, Mach. Learn. (no. 1), vol. 45. doi:doi: 10.1023/A:1010933404324.

Breiman, L., Friedman, J., Olshen, R., & Stone, C. (1984). *Classification and Regression Trees;*. Monterey, CA, USA,: Wadsworth & Brooks/Cole Advanced Books & Software:.

Breiman, L., Friedman, J., Stone, C., & Olshen, R. (1984). Classification and Regression Trees. *Wadsworth & Brooks/Cole Advanced Books & Software:*.

Camargo, F. F., Sano, E. E., Almeida, C. M., Mura, J. C., & Almeida, T. (2019, July 5). A Comparative Assessment of Machine-Learning Techniques for Land Use and Land Cover Classification of the Brazilian Tropical Savanna Using ALOS-2/PALSAR-2 Polarimetric Images. *remote sensing*.

Destaa, H., & Lemma, B. (2017, September 01). SWAT based hydrological assessment and characterization of Lake Ziway sub-watersheds, Ethiopia. *Journal of Hydrology: Regional Studies*.

Dewi, R., Bijker, W., & Stein, A. (2017). Change Vector Analysis to Monitor the Changes in Fuzzy Shorelines. *Remote Sensing., Vol.9*(no. 2). doi: https://doi.org/10.3390/rs9020147

Di Gregorio, A. a. (2000). Land-cover classification: classification concepts and user manual,. *Food and Agriculture Organization (FAO) of the United Nations Rome.*

Dinka M.O., Chaka D.D. (2019). Analysis of land use/land cover change in Adei watershed, Central Highlands of Ethiopia. *Journal of water and land development, No. 41 (IV–VI)*, p. 146–153. doi:DOI: 10.2478/jwld-2019-0038.

DINKA, M. O., & Chaka, D. D. (2019). Analysis of land use/land cover change in Adei watershed, Central Highlands of Ethiopia. *Jornal of water and land development*(No. 41 (IV–VI)), p. 146–153. doi:DOI: 10.2478/jwld-2019-0038.

Ernani, Z., & Gabriels, D. (2006). Detection of land cover changes using Landsat MSS,TM, ETM + Sensors in Yazd-Ardkan basin, Iran. *Proceedings of Agro Environ*, PP.513–519.

FAO. (2012). *State of the World"s Forest.* Rome, Italy.

Farda, N. M. (2017). Multi-temporal Land Use Mapping of Coastal Wetlands Area using Machine Learning in Google Earth Engine. *IOP Conference Series: Earth and Environmental Science.The 5th Geoinformation Science Symposium.* IOP Publishing Ltd. doi:doi :10.1088/1755-1315/98/1/012042

Fentie, S. F., Jembere, K., Fekadu, E., & Dessale, W. (2020, September 1). Land Use and Land Cover Dynamics and Properties of Soils under Different Land Uses in the Tejibara Watershed, Ethiopia. (P. C. McGuire, Ed.) *Hindawi the Scientific World Journal*.

Ferrari, M. (2019, November 1). A Panoptic Cartography of Remote Sensing. P.132-142.

Frauke Degenhardt, S. S. (2019, March). Evaluation of variable selection methods for random forests and omics data sets. *Briefings in Bioinformatics,, Volume 20,* (Issue 2,), Pp. 492–503,. doi: https://doi.org/10.1093/bib/bbx124

Ganasri, B. a. (2015). Study of Land Use/Land Cover Dynamics through Classification Algorithms for Harangi Catchment Area, K. *Aquatic Procedia,*, P.1413-1420. doi: https://doi.org/10.1016/j.aqpro.2015.02.183

Gebeyehu, M. N. (2019, May). Remote Sensing and GIS Application in Agriculture and Natural Resource Management. *International jornal of Environmental and natural resources, V.19*(2).

Gebre, T. K., Tesfaye, S., & Taye, G. (2015, April). Analysis of Watershed Attributes for Water Resources Management Using GIS: The Case of Chelekot Micro-Watershed, Tigray, Ethiopia. *Journal of Geographic Information System, Vol.7* (No.2).

Geetha, M., Ashagowda, K., & Sudhira, S. (2019, September). Land Use and Land Cover Mapping of Davangere using Google Earth Engine. *International Journal of Recent Technology and Engineering (IJRTE), Volume-8*(Issue-3).

Githu. (2009). Assessing the impacts of environmental change on the hydrology of the Nzoia catchment, in the Lake Victoria Basin. *Department of Hydrology and Hydraulic* .

Goldblatt, R., Rivera Ballesteros, A., & Burney, J. (2017). High Spatial Resolution Visual Band Imagery Outperforms Medium Resolution Spectral Imagery for Ecosystem Assessment in the Semi-Arid Brazilian Sertão. *Remote Sens*.

Gonfa. (1996). Climate classification of Ethiopia. Addis Ababa, Ethiopia. .

Google EarthEngine. (2012). Retrieved February 5, 2014, from https://earthengine.google.org/#intro.

Gorelick, N. H. (2017). Google Earth Engine: Planetary-scale geospatial analysis for everyone. *Remote Sensing ofEnvironment*,, 18-27.

Gorelick, N., Hancher, M., Dixon, M., Ilyushchenko, S., Thau, D., & Moore, R. (2017). Google Earth Engine: Planetary-scale geospatial analysis for everyone. *Remote Sensing of Environment*, pp. 18-27. doi:DOI: 10.1016/j.rse.2017.06.031.

Gustav Tolt, M. S. (2011, July). data, A shadow detection method for remote sensing images using VHR hyperspectral and LIDAR. *IEEE International Geoscience and Remote Sensing Symposium, IGARSS 2011*,, (pp. july 24-29, 2011). Vancouver, BC, Canada, J. doi:10.1109/IGARSS.2011.6050213

Hargreaves, G. &. (1985). Reference crop evapotranspiration from Temperature. . *Applied Engineering in Agriculture* , pp.96-99.

Hayes, T., Usami, S., Jacobucci, R., & McArdle, J. (2015). Using Classification and Regression Trees (CART) and random forests to analyze attrition: Results from two simulations. *Psychol. Aging*, P.911-929.

Haykin, S. (2008). *Neural Networks and Learning Machines.* (3rd ed. ed.). United States of America,.

Herrera, V. K. (2019, July 30). Random forest implementation and optimization for Big Data analytics on LexisNexis's high performance computing cluster platform. *journal of Big Data*. doi:https://doi.org/10.1186/s40537-019-0232-1

Heuvelmans, G. M. (2004). Analysis of the spatial variation in the parameters of the SWAT model with application in Flanders, Northern Belgium,. *Hydrol. Earth Syst. Sci.,, V.8*, P.931–939.

Ho, T. K. (1998). *The random subspace method for constructing decision forests.* (Vol. 20). IEEE Trans. Pattern Anal. Mach. Intell. doi: doi: 10.1109/34.709601

Isabela Xavier Floreano, L. A. (2021, March 30). Land use/land cover (LULC) analysis (2009–2019) with Google Earth Engine and 2030 prediction using Markov-CA in the Rondônia State, Brazil. *Environ Monit Assess*.

Jamsran, B.-E., Lin, C., Byambakhuu, I., Raash, J., & Akhmadi, K. (2019). Applying a support vector model to assess land cover changes in the Uvs Lake Basin ecoregion in Mongolia. *Information processing in agriculture* , pp.158–169.

JeganathanI, C., P. K., K. G., Garg, R. D., Sinha, A. K., Avisek, K., & Hebbale, R. (2017). REMOTE SENSING AND GIS FOR CIVIL engineering applications and human development. *International Journal of Advancement in Remote Sensing, GIS and Geography, Vol.5,* (No.1,), v. 1-18.

Jensen, J. (2003). Introductory image processing: A remote sensing perspective. pp.467-494.

Jha, M. (2011). Evaluating hydrologic response of an agricultural watershed for watershed analysis. Water 3, 604–617.

Kabir Uddin , Mir Abdul Matin and Sajana Maharjan. (2018). Assessment of Land Cover Change and Its Impact on Changes in Soil Erosion Risk in Nepal. *Sustainability*, 1-20.

Khorram, N. S. (2013). *Handbook of Satellite Applications.* (M. S.-L. Pelton J.N., Ed.) Springer, New York, NY.: Digital Image Acquisition: Preprocessing and Data Reduction. doi:https://doi.org/10.1007/978-1-4419-7671-0_46

Kinati Chimdessa, S. Q. (2018, December 26). Effect of Land Use Land Cover and Climate Change on River Flow and Soil Loss in Didessa River Basin, South West Blue Nile, Ethiopia.

Lambin, E. ,. (2003, July 16). Dynamics of land-use and land-cover change in tropical regions. *Annu. Rev. Environ. Resour.*

Legates D.R and McCabe Jr., G. (1999). Evaluating the use of "goodness-of-fit" measures in hydrologic and hydroclimatic model validation. *Water Resour. Res. 35 (1), 233–241.*

Lenhart etal. (2002). Modeling response of soil erosion and runoff to change in precipitation and cover. *Tucson,AZ 85719, USA: USDA-ARS Southwest Watershed Management Research Center.*

Lillesand, T. M. (2004). *Remote sensing and Image interpretation* (5th ed.). New York: .John and Sons, Inc.

Lillesand, T., Kiefer, R., & Chipman, J. (2004). *Remote Sensing and Image Interpretation* (5th ed.). New York.: John Wiley & sons, Inc.

Lin, C., JunMin, L., & XiaoXue, L. (2010). Application of Support Vector Machine in the groundwater quality evaluation. *Journal of Northwest A & F University - Natural Science, Vol.38* , pp.221-226 . Retrieved from http://www.xnxbz.net/.../index.aspx

Lin, C., Wu, C.-C., Tsogt, K., Ouyang, Y.-C., & Chang, C.-I. (2015, February 9). Effects of atmospheric correction and pansharpening on LULC classification accuracy using WorldView-2 imagery. *Information processing in agriculture*, pp. 25-36.

Liu, C.-C., Shieh, M.-C., Ke, M.-S., & Wang, K.-H. (2018). Flood Prevention and Emergency Response System Powered by Google Earth Engine. *Remote Sens.*(10, 1283.).

Liu, R. C. (2016, August). Assessing spatial likelihood of flooding hazard using naïve Bayes and GIS: a case study in Bowen Basin, Australia. *Stoch Environ Res Risk Assess 3*, PP.1575–1590 . doi: https://doi.org/10.1007/s00477-015-1198-y

Lobo, F., Souza-Filho, P., Novo, E., Carlos, F., & Barbosa, C. (2018). Mapping Mining Areas in the Brazilian Amazon Using MSI/Sentinel-2 Imagery (2017). *Remote Sens.*(10, 1178.).

Luigi Barazzetti, M. S. (2014). Automatic Co-registration of Satellite Time Series via Least Squares Adjustment. *European Journal of Remote Sensing, 47*(1), 55-74,. doi: DOI: 10.5721/EuJRS20144705

Mallupattu, P. K., & Reddy, J. R. (2013). Analysis of Land Use/Land Cover Changes Using Remote Sensing Data and GIS at an Urban Area, Tirupati, India. *The Scientific World Journal*. doi:http://dx.doi.org/10.1155/2013/268623

Marchant, R., Richer, S., Boles, O., Capitani, C., Courtney-Mustaphi, C., Lane, P., . . . al, e. (2018). Drivers and trajectories of land cover change in East Africa: Human and environmental interactions from 6000 years ago to present. *Earth Sci. Rev.*(178), 322–378.

Masoud, M., Bahram, S., Fariba, M., & Mahdi, M. (2017, May). Random forest wetland classification using ALOS-2 L-band, RADARSAT-2C-band, and TerraSAR-X imagery. *ISPRS Journal of Photogrammetry and Remote Sensing*, PP.13-31.

Mateo-García, G., Gómez-Chova, L., Amorós-López, J., Muñoz-Marí, J., & Camps-Valls, G. (2018). Multitemporal Cloud Masking in the Google Earth Engine. *Remote Sens.*(10, 1079.).

Melesse, A. M., Weng, Q., S.Thenkabail, P., & Senay, G. B. (2007, December 11). Remote Sensing Sensors and Applications in Environmental Resources Mapping and Modelling. *sensors* .

Mendelsohn, R. (2011). Climate Change. In G. K. Ingram, & Y.-H. Hong (Ed.), *ISBN 978-1-55844-217-7.* the Lincoln Institute of Land Policy.

Mondal, P., Liu, X., Fatoyinbo, T. E., & Lagomasino, D. (2019, December 6). Evaluating Combinations of Sentinel-2 Data and Machine-Learning Algorithms for Mangrove Mapping in West Africa. *remote sensing*.

Monteith, L. (1965). Evaporation and the environment. In The state and Movement Of water in living organisms. *19th Symposia of the Society for Experimental Biology* (pp. pp. p. 205-234). London, U.K.: Cambridge University, Press.

Msofe, N. K., Sheng, L., & Lyimo, J. (2019, January 18). Land Use Change Trends and Their Driving Forces in the Kilombero Valley Floodplain, Southeastern Tanzania. *sustainability* .

Mutanga, O., & Kumar, L. (2019). Google Earth Engine Applications. *Remote Sensing, 11*(5). doi: DOI: 10.3390/rs11050591

Naghibi, S. A. (2017, April 19). Application of Support Vector Machine, Random Forest, and Genetic Algorithm Optimized Random Forest Models in Groundwater Potential Mapping. *Water Resour Manage , 31,,* PP. 2761–2775. doi: https://doi.org/10.1007/s11269-017-1660-3

Nash, J. a. (1970). River flow forecasting through conceptual models part I—a discussion of principles. *J. Hydrol. 10 (3), 282–290.*

Navarro, J. A. (2017). First Experiences with Google Earth Engine. *Conference Paper ·*. doi:DOI: 10.5220/0006352702500255

Neetu, & Ray, S. S. (2019). Exploring Machine Learning Classification Algorithms for Crop Classification Using Sentinel 2 Data. *The International Archives of the Photogrammetry, Remote Sensing and Spatial Information Sciences,, V. XLII-3/W6,*

Negese, A. (2021, February 16). Impacts of Land Use and Land Cover Change on Soil Erosion and Hydrological Responses in Ethiopia. (T. M. Miano, Ed.) *Applied and Environmental Soil Science*.

Neitsch, S. L. (2011). Soil and water assessment ool theoretical documentation version 2009. *Texas Water Resources Institute.* .

Nurfadila, J. S., S. B., Neswati, R., Rukmana, D., & Zylshal, Z. (2019). Initial Results on Landuse/Landcover Classification Using Pixel-Based Random Forest Algorithm on Sentinel-2 Imagery over Enrekang Region. *IOP Conference Series: Earth and Environmental Science.*

Oliphant, A. J., Thenkabail, P. S., Teluguntla, P., Xiong, J., Gumma, M. K., Congalton, R. G., & Yadav, K. (2019, May 22). Mapping cropland extent of Southeast and Northeast Asia using multi-yeartime-series Landsat 30-m data using a random forest classifier on the GoogleEarth Engine Cloud. *Int J Appl Earth Obs Geoinformation*, pp.110-124.

Poortinga, A., Clinton, N., Saah, D., Cutter, P., Chishtie, F., Markert, K., . . . Tran, L. (2018). An Operational Before-After-Control-Impact (BACI) Designed Platform for Vegetation Monitoring at Planetary Scale. *Remote Sens.*

Priestley, C., & Taylor, R. (1972). The assessment of surface heat flux and Evaporation using large-scale parameters. *Mon. Weather Rev*, pp.81-92.

Ratika Pradhan, M. K. (2010, October). Land Cover Classification of Remotely Sensed Satellite Data using Bayesian and Hybrid classifier. *International Journal of Computer Applications ·, V. 7*.

Ray, S. S. (2019, July). EXPLORING MACHINE LEARNING CLASSIFICATION ALGORITHMS FOR CROP CLASSIFICATION USING SENTINEL 2 DATA. *Mahalanobis National Crop Forecast Centre, V. XLII-3*. doi:DOI: 10.5194/isprs-archives-XLII-3-W6-573-2019

Robin Genuer, J.-M. P.-M. (2010). Variable selection using Random Forests. *Pattern Recognition Letters,*, pp.2225-2236.

Rodriguez-Galiano, V. F., Ghimire, B., Rogan, J., & Rigol-Sanchez, J. P. (2012, January). An assessment of the effectiveness of a random forest classifier for land-cover classification. *Journal of Photogrammetry and Remote Sensing*, 93–104. doi:DOI: 10.1016/j.isprsjprs.2011.11.002

Rowcroft, P. (2005). . Gaining Ground: The Socio-Economic Driving Forces Behind Decisions Regarding Land Use and Land change; An Overview, Working Paper 16: Vientiane, Loas,.

Roy. P. S. and Roy.A. (2010). Land use and land cover change in India: A remote sensing & GIS prespective. *Journal of the Indian Institute of Science, VOL 90:4*.

Rudrapal, D., & Subhedar, M. S. (2015, ,September). Land Cover Classification using Support Vector Machine. *International Journal of Engineering Research & Technology (IJERT), Vol. 4* (Issue 09).

Sahoo, B. J. (2019). Application of Support Vector Regression for Modeling Low Flow Time Series. *KSCE J Civ Eng*(23), pp.923–934. doi:https://doi.org/10.1007/s12205-018-0128-1

Sazib, N., & Bolten, I. M. (2018). Leveraging Google Earth Engine for Drought Assessment using Global Soil Moisture Data . *Remote sensing* .

Serrano, J., Shahidian, S., & Silva, J. M. (2019, January 1). Evaluation of Normalized Difference Water Index as a Tool for Monitoring Pasture Seasonal and Inter-Annual Variability in a Mediterranean Agro-Silvo-Pastoral System. *water*.

Setegn, S. G. (2008). Hydrological modelling in the Lake Tana Basin, Ethiopia using SWAT model. *The Open Hydrology Journal,* , 49-62.

Shaohong, T., Xianfeng, Z., Jie, T., & Quan, S. (2016, November 16). Random Forest Classification of Wetland Landcovers from Multi-Sensor Data in the Arid Region of Xinjiang, China. *remote sensing*.

Shi, D., & Yang, X. (2015, January). Support Vector Machines for Land Cover. *A Geomatics Perspective, Springer Remote Sensing/Photogrammetry,*.

Shivangi Mishra, P. S. (2017). Change Detection Techniques in Remote Sensing: A Review. *International Journal of Wireless and Mobile Communication for Industrial Systems, Vol. 4,* (No. 1), pp. 1-8.

Sidhu, N., Pebesma, E., & Câmara, G. (2018). Using Google Earth Engine to detect land cover change: Singapore as a use case. *EUROPEAN JOURNAL OF REMOTE SENSING,, VOL. 51,* (NO. 1,), PP.486–500.

Sime, F. G. (2020, November 3). Stream fow modeling using SWAT model and the model performance evaluation in Toba sub-watershed, Ethiopia. *Modeling Earth Systems and Environment*.

Singh, A. (1989). Review article Digital chaenge detection techniques using remotely sensed data. *International journal of remote sensing*, 989-1003.

Siroky, D. S. (2009). Navigating Random Forests and related advances in algorithmic modeling. *Statistics Surveys, Vol. 3* , pp.147–163. doi:DOI: 10.1214/07-SS033

Somvanshi, S., PhoolKunwar, & Singh, M. (2018, January). Remote Sensing And Gis Techniques for Sustainable Land Resource Management And Planning. *International Refereed Journal of Engineering and Science (IRJES), Volume 7*(Issue 1), PP. 11-24.

Sproles, E., Crumley, R., Nolin, A., Mar, E., & Lopez Moreno, J. (2018). SnowCloudHydro—A New Framework for Forecasting Streamflow in Snowy, Data-Scarce Regions. *Remote Sens., 10* .

Sun, C., Liu, G., & Sha, X. (2016, August 5). Land-Use Conversion Changes the Multifractal Features of Particle-Size Distribution on the Loess Plateau of China. *International Journal of Environmental Researchand Public Health*.

Sunmin, L., Kim, J.-C., Jung, H.-S., Lee, M. J., & Lee, S. (2017, March 8). Spatial prediction of flood susceptibility using random-forest and boosted-tree models in Seoul metropolitan city, Korea. *Geomatics, Natural Hazards and Risk*. doi: https://doi.org/10.1080/19475705.2017.1308971

Taalab, K., Cheng, T., & Zhang, Y. (2018). Mapping landslide susceptibility and types using Random Forest. *Journal of bige earth data, Volume 2*, (Issue 2).

Taati, A., Sarmadian, F., Mousavi, A., Pour, C. T., & Shahir, A. H. (2015, March). Land Use Classification using Support Vector Machine and Maximum Likelihood Algorithms by Landsat 5 TM Images. *Engineering and Physical Sciences*.

Tadesse, L., Suryabhagavan, K., Sridhar, G., & Legesse, G. (2017, May 11). Land use and land cover changes and Soil erosion in Yezat Watershed, North Western Ethiopia. *International Soil and Water Conservation Research*.

Tegene, B. (2002). Land-Cover/Land-Use Changes in the Derekolli Catchment of. *Eastern Africa Social Science Research Review, V.18*.

Temesgen Gashaw, Y. T. (2021). Evaluating the Effectiveness of Best Management Practices On SoilErosion Reduction Using the SWAT Model: for the Case of GumaraWatershed, Abbay (Upper Blue Nile) Basin. *Environmental Management, 68*, 240–261.

Tewabe.D and Fentahun.T. (2020). Assessing land use and land cover change detection using remote sensing in the Lake Tana Basin, Northwest Ethiopia. *Cogent Environmental Science, Vol.6:1*.

Tingting Dan, Y. Y. (2018, July 5). Multi-Temporal Remote Sensing Image Registration Using Deep Convolutional Features. *IEEE*.

Tsai, Y., Stow, D., Chen, H., Lewison, R., An, L., & Shi, L. (2018). Mapping Vegetation and Land Use Types in Fanjingshan National Nature Reserve Using Google Earth Engine. *Remote Sens.*

Vapnik, V. (1999). An overview of statistical learning theory. *IEEE Trans. Neural Netw., V.10*, 988–999.

Wagle, N., Acharya, T., Kolluru, V., Huang, H., & Lee, D. (2020). Multi-Temporal Land Cover Change Mapping Using Google Earth Engine and Ensemble Learning Methods. *Applied Sciences. , 10(22):8083.* doi: https://doi.org/10.3390/app10228083

Wahap, N., & Shafri, H. Z. (2020). Utilization of Google Earth Engine (GEE) for land cover monitoring over Klang Valley, Malaysia. *IOP Conf. Series: Earth and Environmental Science*.

Waranyu, B. a. (2016, January 19). DEM Resolution Impact on the Estimation of the Physical Characteristics of Watersheds by Using SWAT. *Advances in Civil Engineering*.

Wubie. (2015, May). GIS and Remote Sensing Based Forest Change Detection For Sustainable Forest Management In Bench Maji Zone, Ethiopia. *International Journal of Remote Sensing & Geoscience (IJRSG)*.

Wubie, M. A., & Melania, D. (2016). Patterns, causes and consequences of land use/cover dynamics in the Gumara watershed of Lake Tana basin, north western. *remoste sesing*.

Xiaolu, S., & Bo, C. (2011). Change Detection Using Change Vector Analysis from . *Procedia Environmental Sciences* , pp.238 – 244.

Xiong, J., Thenkabail, P. S., Gumma, M. K., Teluguntla, P., J. P., Congalton, R. G., . . . D. T. (2017, March 8). Automated cropland mapping of continental Africa using Google Earth Engine cloud computing. *Journal of Photogrammetry and Remote Sensing*, PP. 225 -244.

Xiong, J., Thenkabail, P., Tilton, J., Gumma, M., Teluguntla, P., Oliphant, A., . . . Gorelick, N. (2017). Nominal 30-m Cropland Extent Map of Continental Africa by Integrating Pixel-Based and Object-Based Algorithms Using Sentinel-2 and Landsat-8 Data on Google Earth Engine. *Remote Sens.* .

Y. H. Tsai, D. S. (2018, Jun 12). Mapping Vegetation and Land Use Types in Fanjingshan National Nature Reserve Using Google Earth Engine. *Remote Sens.* doi:doi:10.3390/rs10060927

Yang, X., & Lo, C. P. (2001, Nov 25). Using a time series of satellite imagery to detect land use and land cover changes in the Atlanta,Georgia metropolitan area. *International Journal of Remote Sensing*.

Yoon, H.-K. (2011, April). Human modification of korean landforms for geomantic purposes. *Geographical Review, Vol. 101*(No. 2), pp. 243-260.

Zaitunah, A., Samsuri, S., Ahmad, A. G., & Safitri, R. A. (2018, March). Normalized difference vegetation index (ndvi) analysis for land cover types using landsat 8 oli in besitang watershed, Indonesia. *IOP Conference Series Earth and Environmental Science*. doi:: 10.1088/1755-1315/126/1/012112

Zakariah, M. (2014, September). Classification of large datasets using Random Forest Algorithm in various applications: Survey. *International Journal of Engineering and Innovative Technology (IJEIT), Volume 4*(Issue 3).

Zurqani, H., Post, C. J., Mikhailova, E., Cope, M. P., S.Allen, J., & Lytle, B. (2020). *Evaluating the integrity of forested riparian bufers over a large area using LiDAR data andGoogle Earth Engine.*

APPENDICES

APPENDIX A: Google Earth Engine land use land cover mapping codes

```
* Function to mask clouds based on the pixel_qa band of Landsat SR data.
 * @param {ee.Image} image Input Landsat SR image
 * @return {ee.Image} Cloudmasked Landsat image
 */
var cloudMaskL457 = function(image) {
  var qa = image.select('pixel_qa');
  // If the cloud bit (5) is set and the cloud confidence (7) is high
  // or the cloud shadow bit is set (3), then it's a bad pixel.
  var cloud = qa.bitwiseAnd(1 << 5)
                .and(qa.bitwiseAnd(1 << 7))
                .or(qa.bitwiseAnd(1 << 3));
  // Remove edge pixels that don't occur in all bands
  var mask2 = image.mask().reduce(ee.Reducer.min());
  return image.updateMask(cloud.not()).updateMask(mask2);
};
var image = ee.ImageCollection("LANDSAT/LT05/C01/T1_SR")
          .filterBounds(ROI)
          .filterDate('1986-11-01', '1986-12-28')
          .map(cloudMaskL457)
          .filterMetadata('CLOUD_COVER', 'less_than', 5)
          .first()
Map.centerObject(ROI,11);
var vizParams2 = {bands: ['B3', 'B2', 'B1'], min: 0, max: 3000, gamma: 1.4,};
Map.addLayer(image.clip(ROI), vizParams2, 'TRUE Landsat 1986');
vartraining_points=GrasLand.merge(Vegetation).merge(BareLand).merge(AGRICULTUR
ALLand).merge(ShurebLand).merge(MixedLand);
var bands = ['B2', 'B3', 'B4', 'B5', 'B6', 'B7'];
```

```
var points = ee.FeatureCollection(training_points);
print(training_points);
var train_sam = image.select(bands).sampleRegions({
    collection: points,
    properties: ["LC"],
    scale: 30
});
// delet the nul
// Filter out the null property values and try again.
var trainingNoNulls =  train_sam.filter(
  ee.Filter.notNull( train_sam.first().propertyNames())
);
var trained = ee.Classifier.smileRandomForest(10).train(trainingNoNulls , 'LC', bands);
var classified = image.select(bands).classify(trained);
Map.addLayer(classified.clip(ROI),
            {min: 0, max: 3, palette: ['#821dd6', '#12ff14', '#e5f727', '#ff3a14', '#00f5f5',
'#16d620']},
            'classification 1986');
            print(trained.confusionMatrix().kappa(), 'kappa');
print(trained.confusionMatrix(), 'matrix');
// Convert lulc raster to polygons
var FLULC_vec = classified.reduceToVectors({
  scale: 30,
  geometryType:'polygon',
  geometry:ROI,
  maxPixels: 1e9,
  eightConnected: false,
  bestEffort:true,
  tileScale:4,
```

```
});
// Export LULC polygons as shape-file
Export.table.toDrive({
  collection:FLULC_vec,
  description:'FLULC_vec_shp',
  fileFormat:'SHP',
  fileNamePrefix:'FLULC_vec'
});
//Export the raster dataset
Export.image.toDrive({
  scale: 10,
  image: classified,
  description: 'LC_raster',
  fileNamePrefix: 'lulc',
  region:ROI,
  maxPixels: 1e8
});
//Areal coverage of land use land cover class (km2)
var area_1986 = ee.Image.pixelArea().divide(1000*1000).addBands(classified.clip(ROI))
    .reduceRegion({
    reducer: ee.Reducer.sum().group({
      groupField: 1,
      groupName: 'code',
    }),
    geometry: ROI,
    scale: 30,
    maxPixels:1e9
}).get('groups');
print('Kulfo km2 (2016):', area_1986);
```

//SECTION 2 - Kulfo 2020

```
var image = ee.Image(ee.ImageCollection('LANDSAT/LC08/C01/T1_SR')
        .filterBounds(ROI)
        .filterDate('2020-12-01', '2020-12-28')
        .filterMetadata('CLOUD_COVER', 'less_than', 1)
        .first())
Map.centerObject(ROI,11);
var vizParams2 = {bands: ['B4', 'B3', 'B2'], min: 0, max: 3000, gamma: 1.4,};
Map.addLayer(image.clip(ROI), vizParams2, 'TRUE Landsat 2020');
var training_points = BareLand.merge(AgriculturalLand).merge(vEGITATION).merge(shrubland).merge(Grass land).merge(Cloude);
var bands = ['B2', 'B3', 'B4', 'B5', 'B6', 'B7'];
var points = ee.FeatureCollection(training_points);
print(training_points);
var train_sam = image.select(bands).sampleRegions({
   collection: points,
   properties: ["LC"],
   scale: 30
});
// delet the null
// Filter out the null property values and try again.
var trainingNoNulls =  train_sam.filter(
  ee.Filter.notNull( train_sam.first().propertyNames())
);
var trained = ee.Classifier.smileRandomForest(10).train(trainingNoNulls , 'LC', bands);
var classified = image.select(bands).classify(trained);
Map.addLayer(classified.clip(ROI),
        {min: 0, max: 3, palette: ['#d6d53f', '#ff1450', '#18ff2f', '#00ffff', '#141dc2', '#dcfaf5']},
        'classification 2016');
print(trained.confusionMatrix().kappa(), 'kappa');
print(trained.confusionMatrix(), 'matrix');
```

```
//Validation and training
// Splits data into training and validation groups. Set at 70% training/30% validation
var splitData = function(data){
  var dict = {};
  var randomTpixels = data.randomColumn();
  var trainingData = randomTpixels.filter(ee.Filter.lt('random', 0.7));
  var valiData = randomTpixels.filter(ee.Filter.gte('random', 0.3));
    dict.training = trainingData;
  dict.validation = valiData;
  return dict;
```

APPENDIX B Confusion Matrix using different classifier Algorithms from GEE

Appendix B1 Confusion Matrix using RF Classification

	Bare	Grass Land	Shrub Land	Mixed forest	Agricultural land	Vegetation	**Users Accuracy%**	**Commission error %**
Bare Land	36	0	6	0	6	2	72.0	28.0
Grass Land	5	32	0	1	2	0	80	20
Shrub Land	8	1	41	2	1	0	77.4	22.6
Mixed forest	0	0	0	42	1	0	97.7	2.3
Agricultural land	4	4	4	7	45	1	69.2	30.8
Vegetation	1	0	0	4	1	44	88	12
Sum	54	37	51	56	56	47	80.7	
Producers Accuracy%	66.6667	86.49	80.39	75.00	80.35	93.62		
Omission Error %	33.3333	13.51	19.61	25.00	19.64	6.38		

Appendix B2 Confusion Matrix using Fast Naive Bayes Classification

	Bare Land	Grass Land	Shrub Land	Mixed forest	Agricultural land	Vegetation	**Users Accuracy%**	**Commission error %**
Bare Land	34	0	5	0	11	0	68.0	32.0
Grass Land	0	30	0	1	9	0	75	25
Shrub Land	10	1	31	3	4	4	58.5	41.5

Mixed forest	3	2	1	30	2	5	69.8	30.2
Agricultural land	5	13	0	2	40	5	65.0	35.0
Vegetation	1	1	2	2	9	35	70	30
Sum	53	47	39	38	75	49	67.7	
Producers Accuracy %	64.15	63.83	79.49	78.95	53.33	71.43		
Omission Error %	35.85	36.17	20.51	21.05	46.67	28.57		

Appendix B3 Confusion Matrix using CART Classification

	Bare Land	Grass Land	Shrub Land	Mixed forest	Agricultural land	Vegetation	**Users Accuracy%**	**Commission error %**
Bare	30	0	4	0	14	2	60.0	40.0
Grass Land	2	23	6	0	6	3	57.5	42.5
Shrub Land	10	5	30	2	0	6	56.6	43.4
Mixed forest	4	1	0	30	6	2	69.8	30.2
Agricultural land	5	13	0	9	30	8	65.0	35.0
Vegetation	0	3	0	2	10	35	70	30
Sum	51	45	40	43	66	56	63.1	
Producers%	58.82	51.11	75.00	69.77	45.45	62.50		
Omission Error %	41.18	48.89	25.00	30.23	54.55	37.50		

APPENDIX C: LULC map of the Kulfo catchment that were classified using four different algorithms

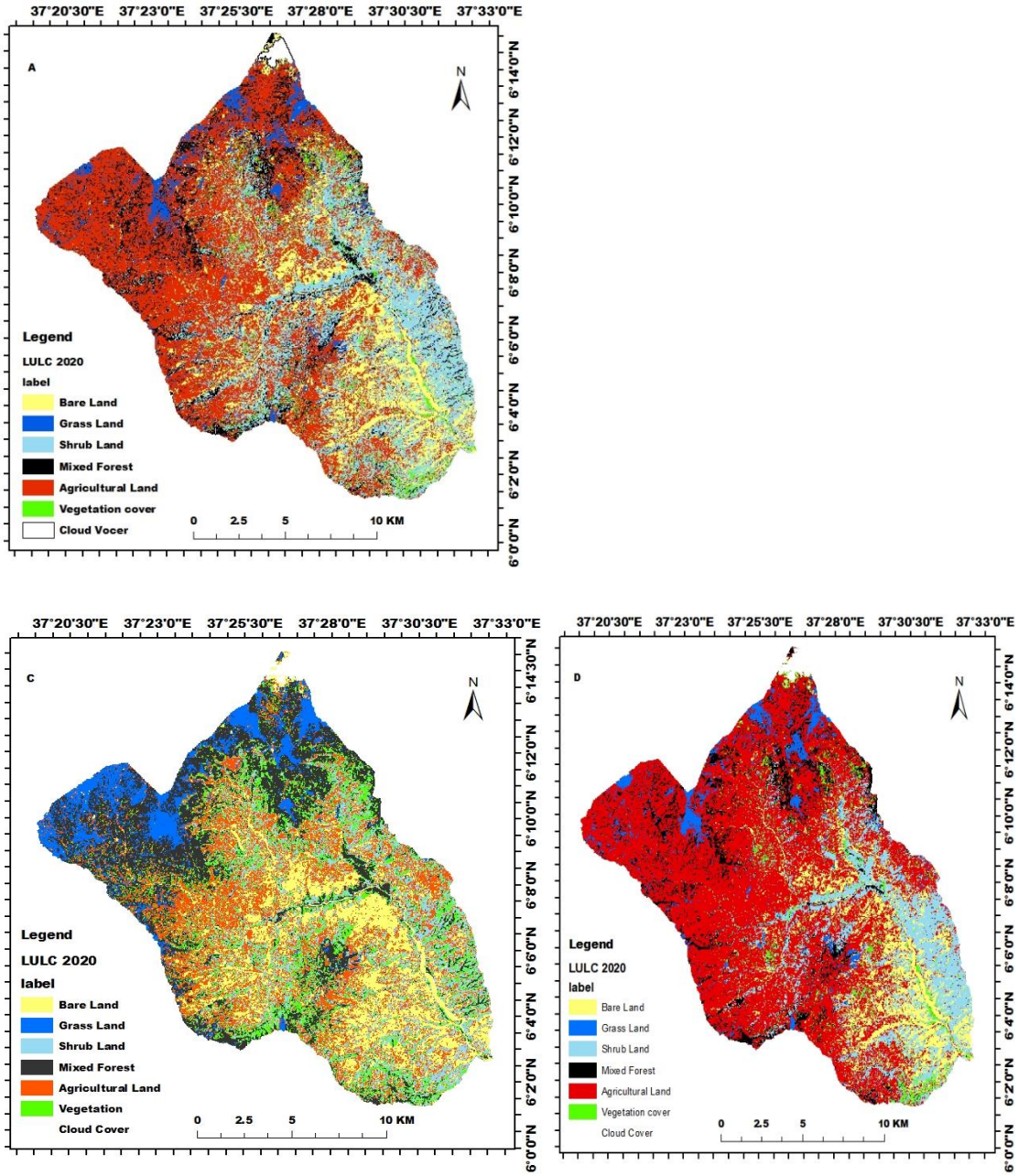

Figure XXX Land cover maps of Kulfo catchment that were generated using (A) SVM, (B) RF, (C) Fast Naive Bayes and (D) CART machine learning algorithms using Landsat OLI image collected at the date of 2020 – 12 -11(https://earthengine.google.com).

APPENDIX D: - Error matrix for classified LULC maps of kulfo catchment A) 1986 B) 2000 and C) 2016

Appendix D1 Error matrix for the 1986 LULC map

	Bare Land	Grass Land	Shrub Land	Mixed Forest	Agricultural Land	Vegetation	Sum	Users Accuracy %	Commission error %
Bare	40	0	5	0	5	0	50	80.0	20.0
Grass Land	0	35	0	1	4	0	40	87.5	12.5
Shrub Land	4	1	45	3	3	3	59	76.3	23.7
Mixed forest	3	2	1	30	2	5	43	69.8	30.2
Agricultural land	3	7	0	2	50	3	65	65.0	35.0
Vegetation	1	1	2	2	4	40	50	80	20
Sum	51	46	53	38	68	51		76.4	
Producers %	78.43	76.09	84.91	78.95	73.53	78.43			240
Omission Error %	21.57	23.91	15.09	21.05	26.47	21.57			
		Over all accuracy = 78.2							
		Kappa coefficient = 0.76							

Appendix D2 Error matrix for the 2000 LULC map

	Bare	Grass Land	Shrub Land	Mixed forest	Agricultural land	Vegetation	Sum	Users Accuracy %	Commission error %
Bare	42	0	3	0	3	2	50	84.0	16.0
Grass Land	5	32	0	1	2	0	40	80	20
Shrub Land	8	1	41	2	1	0	53	77.4	22.6
Mixed forest	0	0	0	42	1	0	43	97.7	2.3
Agricultural land	4	4	4	7	45	1	65	69.2	30.8
Vegetation	1	0	0	4	1	44	50	88	12
Sum	60	37	48	56	53	47			
Producers%	70.00	86.49	85.42	75	84.91	93.62			
Omission Error %	30.00	13.51	14.58	25	15.09	6.38			
		Over all accuracy = 81.73							
		Kappa coefficient = 0.811							

Appendix D3 Error matrix for the 2016 LULC map

	Bare Land	Grass Land	Shrub Land	Mixed forest	Agricultural land		Vegetation	Sum	Users Accuracy %	Commission error %
Bare	45	0	3	0	2		0	50	90.0	10.0
Grass Land	1	37	0	0	2		0	40	92.5	7.5
Shrub Land	3	0	46	3	0		1	53	86.8	13.2
Mixed forest	0	1	3	37	2		0	43	86.0	14.0
Agricultural land	4	3	5	4	50		0	66	75.8	24.2
Vegetation	0	0	1	1	2		46	50	92	8
Sum	53	41	58	45	58		47			
Producers %	84.91	90.24	79.31	82.22	86.21		97.87			
Omission Error %	15.13	9.76	20.7	17.78	13.79		2.13			
		Over all accuracy = 86.71								
		Kappa coefficient = 0.862								

APPENDIX E: Selected sensitive parameters of kulfo watershed

A) Selected sensitive parameters of kulfo watershed using 2000 LULC

No.	Parameter Name	t-Stat	P-Value	Rank
1	V__SURLAG .bsn	-7.688	$8.86*10^{-14}$	1
2	V__GW_DELAY.gw	-6.19	$1.35*10^{-09}$	2
3	R__GW_REVAP.gw	2.73	0.01	3
4	V__REVAPMN.gw	1.83	0.07	4
5	R__SFTMP .bsn	1.63	0.10	5
6	R__RCHRG_DP.gw	-1.21	0.23	6
7	A__SOL_AWC(..).sol	-1.14	0.25	7
8	R__CN2.mgt	-1.12	0.26	8

B) Selected sensitive parameters of kulfo watershed for LULC map of 2016

No.	Parameter Name	t-Stat	P-Value	Rank
1	V__CH_K2.rte	17.05	0.00	1
2	V__ALPHA_BF.gw	-7.33	0.00	2
3	R__CH_ERODMO (...).rte	-1.80	0.07	3
4	V__GW_DELAY.gw	-1.63	0.11	4
6	V__GWQMN.gw	1.59	0.11	5

7	V__SURLAG.bsn	-1.59	0.11	6
8	V__REVAPMN.gw	-1.34	0.18	7
9	R__SOL_ALB (..).sol	-1.17	0.24	8
10	A__SOL_AWC(..).sol	-1.13	0.26	9
11	R__CN2.mgt	1.09	0.28	10
12	V__CH_N2.rte	1.02	0.31	11

C) Selected sensitive parameters of kulfo watershed for the LULC map of 2020

No.	Parameter Name	t-Stat	P-Value	Rank
1	V__GWQMN.gw	-8.50	0.00	1
2	R__CN2.mgt	-7.33	0.00	2
3	V__SURLAG.bsn	-7.22	0.00	3
4	V__GW_DELAY.gw	-3.80	0.00	4
5	R__SOL_ALB (...).sol	-3.58	0.00	5
6	R__SLSUBBSN.hru	-2.42	0.02	6
7	R__CH_N2.rte	1.65	0.10	7
8	R__RCHRG_DP.gw	-1.35	0.18	8
9	R__CH_K2.rte	1.24	0.21	9
10	R__TLAPS.sub	1.13	0.26	10
11	A__SOL_AWC (..).sol	-0.06	0.95	11